CHEMISTRY
A EUROPEAN JOURNAL

DOI: 10.1002/chem.200800430

Coordination Chemistry of Conformation-Flexible 1,2,3,4,5,6-Cyclohexanehexacarboxylate: Trapping Various Conformations in Metal–Organic Frameworks

Jing Wang,[a] Zhuo-Jia Lin,[a] Yong-Cong Ou,[a] Yong Shen,[a] Radovan Herchel,[b] and Ming-Liang Tong*[a]

Abstract: To study the conformations of 1,2,3,4,5,6-cyclohexanehexacarboxylic acid (H_6**L**), eleven new coordination polymers have been isolated from hydrothermal reactions of different metal salts with 1*e*,2*a*,3*e*,4*a*,5*e*,6*a*-cyclohexanehexacarboxylic acid (3e+3a, H_6**L**$^{\mathbf{I}}$) and characterized. They are $[Cd_{12}(\mu_6\text{-}\mathbf{L}^{\mathbf{II}})(\mu_{10}\text{-}\mathbf{L}^{\mathbf{II}})_3(\mu\text{-}H_2O)_6(H_2O)_6]\cdot 16.5\,H_2O$ (**1**), $Na_{12}[Cd_6(\mu_6\text{-}\mathbf{L}^{\mathbf{II}})(\mu_6\text{-}\mathbf{L}^{\mathbf{III}})_3]\cdot 27\,H_2O$ (**2**), $[Cd_3(\mu_{13}\text{-}\mathbf{L}^{\mathbf{II}})(\mu\text{-}H_2O)]$ (**3**), $[Cd_3(\mu_6\text{-}\mathbf{L}^{\mathbf{III}})(2,2'\text{-bpy})_3(H_2O)_3]\cdot 2\,H_2O$ (**4**), $[Cd_4(\mu_4\text{-}\mathbf{L}^{\mathbf{VI}})_2(4,4'\text{-Hbpy})_4(4,4'\text{-bpy})_2(H_2O)_4]\cdot 9.5\,H_2O$ (**5**), $[Cd_2(\mu_6\text{-}\mathbf{L}^{\mathbf{II}})(4,4'\text{-Hbpy})_2(H_2O)_{10}]\cdot 5\,H_2O$ (**6**), $[Cd_3(\mu_{11}\text{-}\mathbf{L}^{\mathbf{VI}})(H_2O)_3]$ (**7**), $[M_3(\mu_9\text{-}\mathbf{L}^{\mathbf{II}})(H_2O)_6]$ (M = Mn (**8**), Fe (**9**), and Ni (**10**)), and $[Ni_4(OH)_2(\mu_{10}\text{-}\mathbf{L}^{\mathbf{II}})(4,4'\text{-bpy})(H_2O)_4]\cdot 6\,H_2O$ (**11**). Three new conformations of 1,2,3,4,5,6-cyclohexanehexacarboxylate, 6e (**L**$^{\mathbf{II}}$), 4e+2a (**L**$^{\mathbf{III}}$) and 5e+1a (**L**$^{\mathbf{VI}}$), have been derived from the conformational conversions of **L**$^{\mathbf{I}}$ and trapped in these complexes by controlling the conditions of the hydrothermal systems. Complexes **1** and **2** have three-dimensional (3D) coordination frameworks with nanoscale cages and are obtained at relatively low temperatures. A quarter of the **L**$^{\mathbf{I}}$ ligands undergo a conformational transformation into **L**$^{\mathbf{II}}$ while the others are transformed into **L**$^{\mathbf{III}}$ in the presence of NaOH in **2**, while all of the **L**$^{\mathbf{I}}$ are transformed into **L**$^{\mathbf{II}}$ in the absence of NaOH in **1**. Complex **3** has a 3D condensed coordination framework, which was obtained under similar reaction conditions as **1**, but at a higher temperature. The addition of 2,2′-bipyridine (2,2′-bpy) or 4,4′-bipyridine (4,4′-bpy) to the hydrothermal system as an auxiliary ligand also induces the conformational transformation of H_6**L**$^{\mathbf{I}}$. A new **L**$^{\mathbf{VI}}$ conformation has been trapped in complexes **4**–**7** under different conditions. Complex **4** has a 3D microporous supramolecular network constructed from a 2D **L**$^{\mathbf{III}}$-bridged coordination layer structure by π-π interactions between the chelating 2,2′-bpy ligands. Complexes **5**–**7** have different frameworks with **L**$^{\mathbf{II}}$/**L**$^{\mathbf{VI}}$ conformations, which were prepared by using different amounts of 4,4′-bpy under similar synthetic conditions. Both **5** and **7** are 3D coordination frameworks involving the **L**$^{\mathbf{VI}}$ ligands, while **6** has a 3D microporous supramolecular network constructed from a 2D **L**$^{\mathbf{II}}$-bridged coordination layer structure by interlayer $N_{4,4'\text{-Hbpy}}$–H···O(**L**$^{\mathbf{II}}$) hydrogen bonds. 3D coordination frameworks **8**–**11** have been obtained from the H_6**L**$^{\mathbf{I}}$ ligand and the paramagnetic metal ions Mn^{II}, Fe^{II}, and Ni^{II}, and their magnetic properties have been studied. Of particular interest to us is that two copper coordination polymers of the formulae $[\{Cu^{II}_2(\mu_4\text{-}\mathbf{L}^{\mathbf{II}})(H_2O)_4\}\{Cu^{I}_2(4,4'\text{-bpy})_2\}]$ (**12**α) and $[Cu^{II}(Hbtc)(4,4'\text{-bpy})(H_2O)]\cdot 3\,H_2O$ (H_3btc = 1,3,5-benzenetricarboxylic acid) (**12**β) resulted from the same one-pot hydrothermal reaction of $Cu(NO_3)_2$, H_6**L**$^{\mathbf{I}}$, 4,4′-bpy, and NaOH. The $Hbtc^{2-}$ ligand in **12**β was formed by the in situ decarboxylation of H_6**L**$^{\mathbf{I}}$. The observed decarboxylation of the H_6**L**$^{\mathbf{I}}$ ligand to H_3btc may serve as a helpful indicator in studying the conformational transformation mechanism between H_6**L**$^{\mathbf{I}}$ and **L**$^{\mathbf{II\text{–}VI}}$. Trapping various conformations in metal-organic structures may be helpful for the stabilization and separation of various conformations of the H_6**L** ligand.

Keywords: conformation analysis · coordination polymers · cyclohexanehexacarboxylate · hydrothermal synthesis · magnetic properties

[a] J. Wang, Dr. Z.-J. Lin, Y.-C. Ou, Dr. Y. Shen, Prof. Dr. M.-L. Tong
MOE Key Laboratory of Synthetic Bioinorganic Chemistry
State Key Laboratory of Optoelectronic Materials and Technologies
School of Chemistry and Chemical Engineering
Sun Yat-Sen University
Guangzhou 510275 (P. R. China)
Fax: (+86) 20-8411-2245
E-mail: tongml@mail.sysu.edu.cn

[b] Dr. R. Herchel
Department of Inorganic Chemistry
Faculty of Sciences, Palacky University
Krizkovskeho 10, 771 47 Olomouc (Czech Republic)

Supporting information for this article is available on the WWW under http://dx.doi.org/10.1002/chem.200800430.

Introduction

When a substrate (L) coordinates to a metal (M) center, the properties of the organic ligand, such as electrophilic or nucleophilic character, acidity, and susceptibility to oxidation or reduction, usually change in tandem with the nature of the metal ion, leading to the production of thermodynamically or kinetically stable coordination compounds.[1] In some cases, reactive transition metal ions can catalyze the oxidation/reduction, rearrangement, or conformational conversion of organic ligands under mild reaction conditions so as to form new ligand derivatives.[2] Hydro(solvo)thermal synthesis has been widely used as an advantageous technique in the preparation of highly stable, infinite metal–ligand frameworks. Furthermore, many interesting metal/organic reactions,[2] such as redox processes of metal ions, and oxidative coupling, hydrolysis, or substitution of ligands, have been found under various hydro(solvo)thermal conditions. We and other groups have developed some in situ ligand syntheses, including copper(II)-mediated oxidative coupling, hydrolysis, substitution, and alkylation of ligands in the course of the construction of novel metal-organic framework materials.[3,4] Such ligand reactions, due to their complexity in terms of mechanisms and their role as a new bridge between inorganic and organic chemistry, require further understanding and investigation.

In the rational design and synthesis of metal-organic frameworks,[5] rigid polycarboxylates, for example benzenepolycarboxylates and pyridinepolycarboxylates, have been extensively employed to produce various extended structures.[6] Nevertheless, only a few coordination polymers based on ligands with flexible conformations have hitherto been reported. This is probably due to the flexibility of the ligand backbones, which makes it more difficult to predict and control their orientation in the final coordination networks.[7] Many investigations have been focused on the flexible 1,4- or 1,3-cyclohexanedicarboxylic acids in view of their *cis*- and *trans*- conformations.[7e,f] 1,2,3,4,5,6-Cyclohexanehexacarboxylic acid (H_6**L**), which is characterized by multiple binding sites and pH-dependent coordination modes and shows versatility through its flexible conformations, has attracted our great interest in studying its conformational transformations and use in constructing metal-organic frameworks.[8] In our recent work on H_6**L**, we have observed two predominant conformations, $\mathbf{L^I}$ (3e+3a) at room temperature and $\mathbf{L^{II}}$ (6e), as well as a less common conformation $\mathbf{L^{III}}$ (4e+2a) under hydrothermal conditions (Scheme 1).[8] It should be noted that the starting material 1,2,3,4,5,6-cyclohexanehexacarboxylic acid hydrate ($H_6\mathbf{L}^{\mathbf{I}}\cdot H_2O$) adopts the all-*cis* conformation with multiple hydrogen bonds, which can be converted in situ to the *trans* form or *cis*,*trans*-mixed forms under different hydrothermal conditions. Conformation $\mathbf{L^I}$ is thermodynamically less stable than the other conformations,[9] but it has relatively low steric hindrance between the carboxylate groups. The opposing factors of the relative energy and steric hindrance result in $H_6\mathbf{L}^{\mathbf{I}}$ adopting various compromised conformations

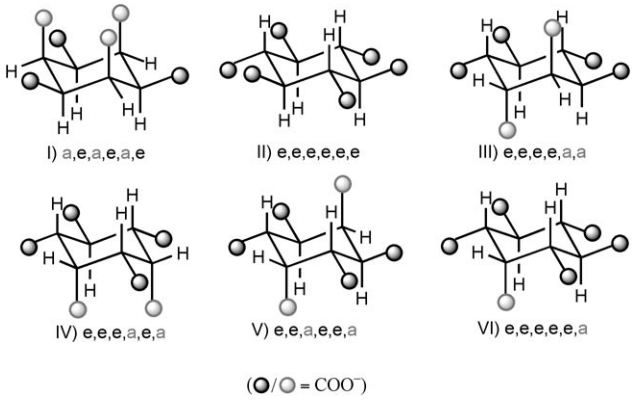

Scheme 1. Possible conformations (**I**–**VI**) of the H_6**L** ligand.

upon coordinating to metal ions, which gives us the opportunity of trapping the intermediate conformations by tuning the hydrothermal reaction conditions. In our ongoing investigation on this interesting metal–H_6**L** system, we have hitherto paid much more attention to the trapping of possible new conformations, for example, 4e+2a and 5e+1a. In the present work, through judicious choice of different hydrothermal reaction conditions, we have successfully obtained seven novel Cd-**L** coordination frameworks, namely $[Cd_{12}(\mu_6\text{-}\mathbf{L^{II}})(\mu_{10}\text{-}\mathbf{L^{II}})_3(\mu\text{-}H_2O)_6(H_2O)_6]\cdot 16.5\,H_2O$ (**1**), $Na_{12}[Cd_6(\mu_6\text{-}\mathbf{L^{II}})(\mu_6\text{-}\mathbf{L^{III}})_3]\cdot 27\,H_2O$ (**2**), $[Cd_3(\mu_{13}\text{-}\mathbf{L^{II}})(\mu\text{-}H_2O)]$ (**3**), $[Cd_3(\mu_6\text{-}\mathbf{L^{III}})(2,2'\text{-bpy})_3(H_2O)_3]\cdot 3.5\,H_2O$ (**4**), $[Cd_4(\mu_4\text{-}\mathbf{L^{VI}})_2(4,4'\text{-Hbpy})_4(4,4'\text{-bpy})_2(H_2O)_4]\cdot 9.5\,H_2O$ (**5**), $[Cd_2(\mu_6\text{-}\mathbf{L^{II}})(4,4'\text{-Hbpy})_2(H_2O)_{10}]\cdot 5\,H_2O$ (**6**), and $[Cd_3(\mu_{11}\text{-}\mathbf{L^{VI}})(H_2O)_3]$ (**7**). Meanwhile, four metal-organic frameworks with paramagnetic metal ions, $[M_3(\mu_9\text{-}\mathbf{L^{II}})(H_2O)_6]$ (M = Mn (**8**), Fe (**9**), and Ni (**10**)) and $[Ni_4(\mu_3\text{-}OH)_2(\mu_{10}\text{-}\mathbf{L^{II}})(4,4'\text{-bpy})(H_2O)_4]\cdot 4\,H_2O$ (**11**), have also been synthesized. Moreover, two new copper coordination polymers have been obtained from the same reaction, green block-shaped crystals of $[\{Cu^{II}_2(\mu_4\text{-}\mathbf{L^{II}})(H_2O)_4\}\{Cu^{I}_2(4,4'\text{-bpy})_2\}]$ (**12**α) and green prismatic crystals of $[Cu(Hbtc)(4,4'\text{-bpy})(H_2O)]\cdot 3\,H_2O$ (H_3btc = 1,3,5-benzenetricarboxylic acid) (**12**β). The $Hbtc^{2-}$ ligand observed in **12**β was formed in situ from the H_6**L** ligand, which may help in understanding the conformational transformations of the $H_6\mathbf{L}^{\mathbf{I}}$ ligand during its reaction processes.

Results and Discussion

Theoretical calculations on the free H_6L ligand in different conformations: Table S1 in the Supporting Information shows that the conformation $\mathbf{L^V}$ is the most stable among the six conformations, which can be rationalized in terms of the formation of a large intramolecular ring of hydrogen bonds involving five -COOH groups. Conformation $\mathbf{L^I}$ is 33.5 and 24.6 kJ mol^{-1} less stable than $\mathbf{L^{II}}$ and $\mathbf{L^{III}}$, respectively. Conformation $\mathbf{L^{II}}$ is the second most stable conformation and conformation $\mathbf{L^{III}}$ is only about 9 kJ mol^{-1} less stable than $\mathbf{L^{II}}$. Obviously, the transformations from $\mathbf{L^I}$ to $\mathbf{L^{II}}$ and from $\mathbf{L^I}$ to $\mathbf{L^{III}}$ should be thermodynamically permitted,

which is in good agreement with the experimental finding that complexes of $\mathbf{L^{II}}$ and $\mathbf{L^{III}}$ can be easily obtained at lower temperature (130 °C). Conformation $\mathbf{L^{VI}}$ is 13 kJ mol^{-1} more stable than $\mathbf{L^{I}}$ and less stable than $\mathbf{L^{II}}$ and $\mathbf{L^{III}}$. Therefore, specific conditions, such as higher temperature (160–180 °C) and the addition of 4,4′-bpy, are required to obtain complexes of conformation $\mathbf{L^{VI}}$. Conformation $\mathbf{L^{IV}}$ is 5 kJ mol^{-1} higher in energy than $\mathbf{L^{I}}$, which indicates that the transformation from $\mathbf{L^{I}}$ to $\mathbf{L^{IV}}$ is thermodynamically restricted, and, indeed, complexes of this conformation could not be obtained from $\mathbf{L^{I}}$ experimentally. The reason why no complex of $\mathbf{L^{V}}$ could be obtained from $\mathbf{L^{I}}$ may be because the hydrogen bonds were destroyed and the conformation was transformed to other forms upon coordination to Cd^{2+}.

Description of the crystal structures

2D/3D Cd^{II}-carboxylate metal-organic frameworks 1–7: Complexes **1** and **2** are composed of 3D metal-organic frameworks (MOFs) with nanoscale cages, and have been reported in our previous work.[8c] In the framework of **1**, the $\mathbf{L^{II}}$ ligands derived from $\mathbf{L^{I}}$ adopt two types of bridging modes, μ_6-$\mathbf{L^{II}}$ and μ_{10}-$\mathbf{L^{II}}$, in a 1:3 ratio (Figure 1a,b). Six μ_{10}-$\mathbf{L^{II}}$ and two μ_6-$\mathbf{L^{II}}$ bridge thirty Cd^{II} atoms to generate a nanoscale $Cd_{36}\mathbf{L^{II}}_8$ cage of hexagonal prism shape of dimensions $22.96 \times 12.81 \times 12.81$ Å^3. Each cage connects six neighboring ones to generate a novel 3D MOF (Figure 1c). Besides the $\mathbf{L^{II}}$ conformation, a new conformation, $\mathbf{L^{III}}$, also derived from $\mathbf{L^{I}}$, is trapped in **2** (Figure 2a,b). This is presumably because of the introduction of Na^{I} atoms, which are directly linked to the neighboring carboxylates within the cages, resulting in different coordination environments of the Cd^{II} atoms from those found for **1**. Both the $\mathbf{L^{II}}$ and $\mathbf{L^{III}}$ ligands adopt μ_6-bridging modes and are present in a 1:3 ratio, connecting the hexagonal prism shaped cages of dimensions $13.04 \times 13.04 \times 10.49$ Å^3 to form a 3D MOF (Figure 2c). An analysis using PLATON[10] suggested that the total void volumes of **1** and **2** without water guests, V_{void}, accounted for 23.9% and 23.1% of the crystal volumes, respectively. The water guests are located in these cages and interact with the MOF host through multiple hydrogen-bonding interactions.

At a higher temperature of 180 °C, a structurally different 3D framework was formed in **3** without the addition of NaOH. A single-crystal X-ray diffraction study revealed that **3** consists of an infinite 3D coordination polymer that recrystallizes in the space group $P\bar{1}$. The asymmetric unit contains three Cd atoms, one deprotonated $\mathbf{L^{II}}$ ligand, and one coordinated water molecule (Figure 3a). Cd1 adopts a slightly distorted octahedral geometry, coordinated by four carboxylate oxygen atoms from different $\mathbf{L^{II}}$ ligands in the equatorial plane (Cd–O 2.186(5)–2.310(4) Å), and one carboxylate atom and a bridging water molecule (Cd–O 2.512(4) and 2.568(5) Å) in the axial positions. Cd2 also has a distorted octahedral geometry, being surrounded by five carboxylate oxygen atoms and a bridging water molecule (Cd–O 2.165(5)–2.355(5) Å). Cd3 adopts a distorted trigonal-bipyrimidal geometry, being coordinated by five carboxylate oxygen atoms (Cd–O 2.174(5)–2.408(4) Å). All of the carboxylate groups of $\mathbf{L^{II}}$ lie in the equatorial positions of the cyclohexane ring, so that the ligand connects thirteen Cd atoms through its six μ-η^1:η^1 and μ_4-η^2:η^2 carboxylate groups. A 3D condensed framework is thus generated by the connection of the μ_{13}-$\mathbf{L^{II}}$ ligands and the bridging water molecules through the cadmium ions (Figure 3b).

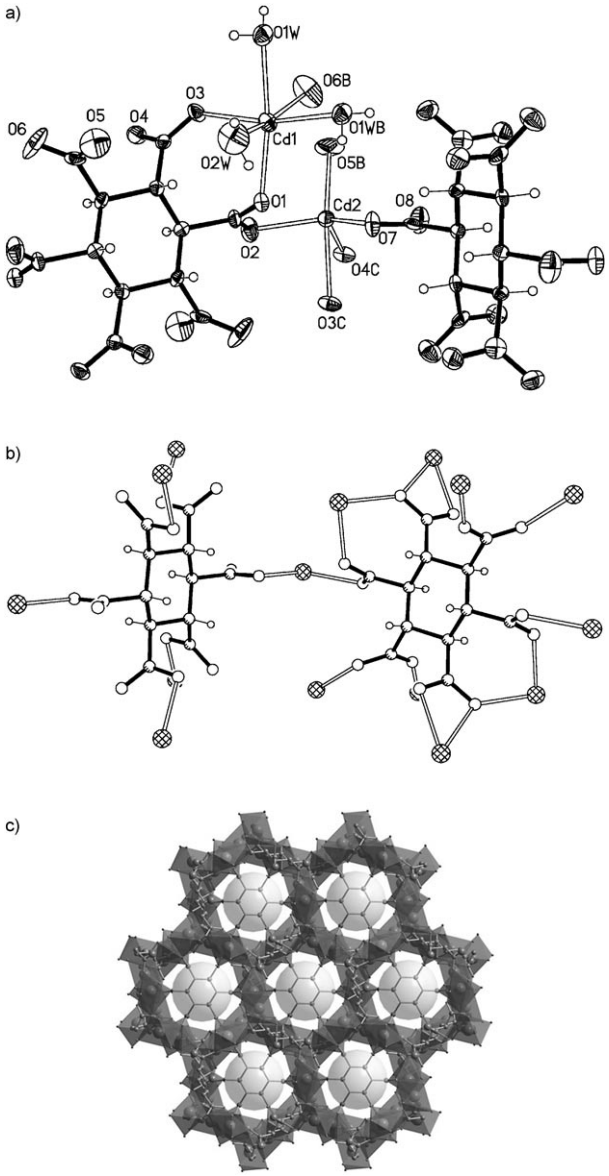

Figure 1. a) ORTEP drawing of the coordination environments of the Cd atoms with thermal ellipsoids at the 50% probability level. Perspective views of b) the coordination mode of the $\mathbf{L^{II}}$ ligand, and c) the 3D MOF with nanoscale cages along the *c* axis in **1**.

In the presence of 2,2′-bpy as an auxiliary ligand, complex **4** with a 2D layered structure was isolated and a new conformation, $\mathbf{L^{III}}$, of the ligand **L** was successfully trapped. X-ray crystallography showed that there are three crystallographically independent Cd atoms, one $\mathbf{L^{III}}$ ligand derived from the $\mathbf{L^{I}}$ conformation, three coordinated water molecules,

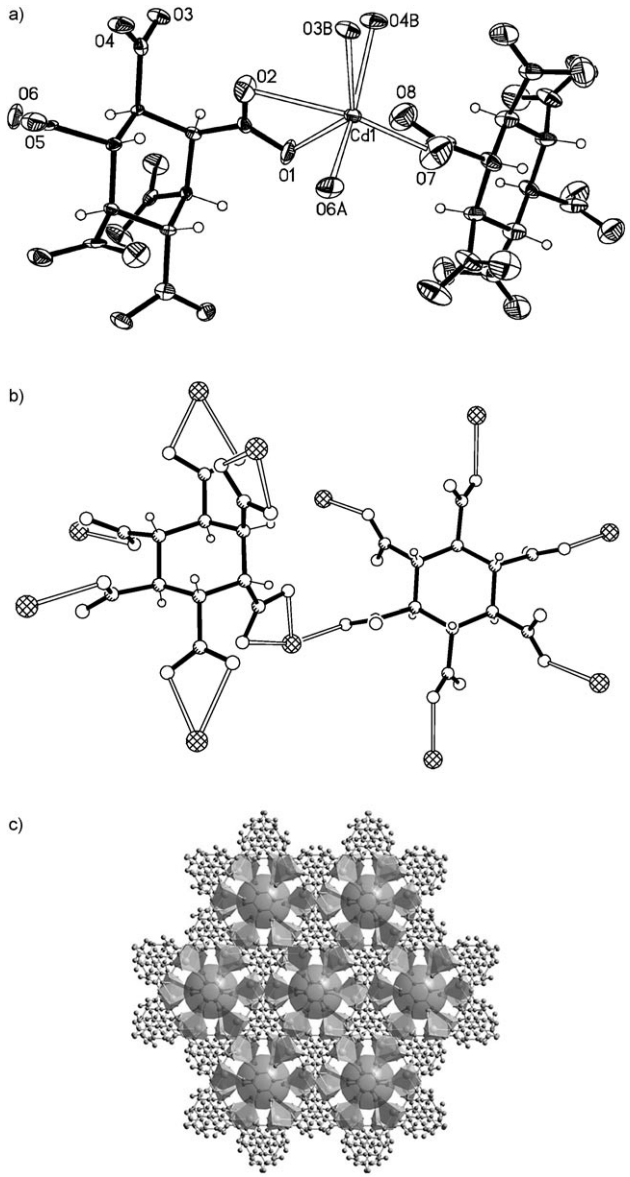

Figure 2. a) ORTEP drawing of the coordination environments of the Cd atoms with thermal ellipsoids at the 50% probability level. Perspective views of b) the coordination mode of the $\mathbf{L^{II}}$ and $\mathbf{L^{III}}$ ligands, and c) the 3D MOF with nanoscale cages along the *c* axis in **2**.

and three-and-a-half disordered lattice water molecules in the structural unit (Figure 4a). Both Cd1 and Cd2 are coordinated by three carboxylate oxygen atoms, one water molecule, and two nitrogen atoms in distorted octahedral environments (Cd–O 2.173(10)–2.475(11) Å, Cd–N 2.302(15)–2.344(12) Å). Cd3 adopts a pentagonal-bipyramidal geometry, coordinated by four carboxylate oxygen atoms, one water molecule, and two nitrogen atoms (Cd–O 2.284(10)–2.575(10 Å, Cd–N 2.327(13) and 2.374(13) Å). In the new conformation $\mathbf{L^{III}}$, the ligand adopts a μ_6-bridging mode connecting six Cd atoms through its one monodentate and four chelating *e*-carboxylate groups and one monodentate *a*-carboxylate group. The μ_6-bridging $\mathbf{L^{III}}$ ligands link the Cd atoms so as to form 2D porous layers (Figure 4b), which are

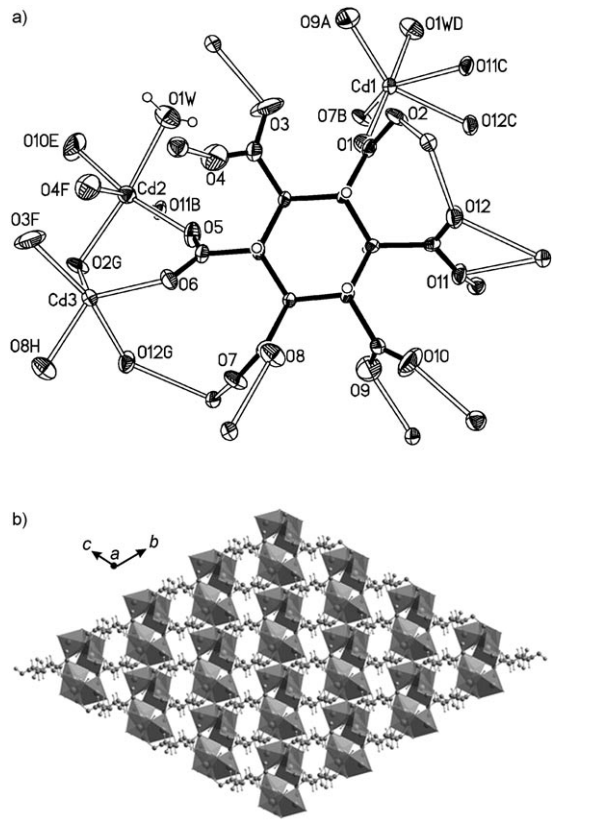

Figure 3. a) ORTEP drawing of the coordination environments of the Cd atoms and the coordination mode of the $\mathbf{L^{II}}$ ligand with thermal ellipsoids at the 50% probability level. b) Polyhedron view of the 3D condensed network in **3**.

further connected to form a 3D supramolecular porous network occupied by lattice water molecules through π–π interactions (3.6 Å) of the 2,2′-bpy ligands and hydrogen bonds between the water molecules and carboxylate groups (Figure 4c).

When the auxiliary chelating ligand 2,2′-bpy was replaced by the divergent bridging ligand 4,4′-bpy, three new complexes, **5**, **6**, and **7**, were obtained under similar hydrothermal conditions (Scheme 2). The reaction of $Cd(NO_3)_2{\cdot}4H_2O$, $H_6\mathbf{L^I}{\cdot}H_2O$, and 4,4′-bpy in a 5:1:5 molar ratio at 160 °C resulted in a complicated 3D coordination framework of **5**. The asymmetric unit contains four crystallographically independent Cd atoms, two $\mathbf{L^{VI}}$ ligands, two bridging 4,4′-bpy,

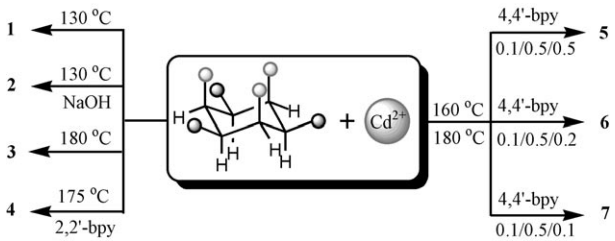

Scheme 2. Summary of the hydrothermal conditions in the preparation of **1**–**7**.

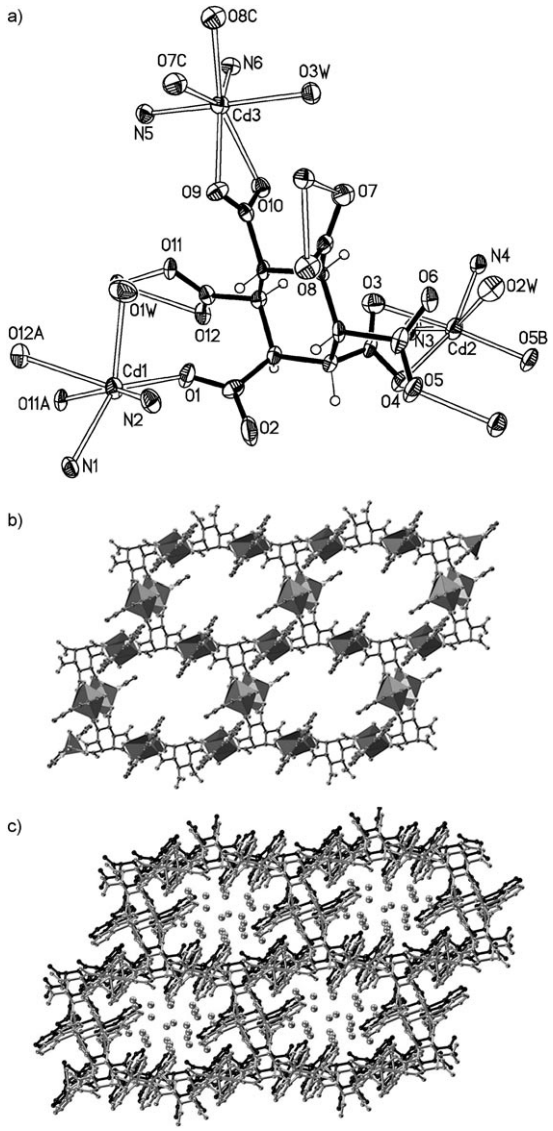

Figure 4. a) ORTEP drawing of the coordination environments of the Cd atoms and the coordination mode of the $\mathbf{L^{III}}$ ligand with thermal ellipsoids at the 50% probability level. Polyhedron view of b) the 2D porous layer, and c) the porous supramolecular network with lattice water molecules in **4**.

four monoprotonated 4,4′-Hbpy, four coordinated water molecules, and nine-and-a-half disordered water molecules. Cd1, Cd2, and Cd3 adopt pentagonal-bipyramidal geometries coordinated by four carboxylate oxygen atoms, one water molecule, and two nitrogen atoms (Cd–O 2.272(9)–2.606(11) Å, Cd–N 2.296(10)–2.352(10) Å). Cd4 is in a distorted octahedral environment surrounded by three carboxylate oxygen atoms, one water molecule, and two nitrogen atoms (Cd–O 2.199(12)–2.447(9) Å, Cd–N 2.326(9) and 2.357(9) Å) (Figure 5a). Similar to complex **4** with $\mathbf{L^{III}}$, not $\mathbf{L^{VI}}$ in **4**, the $\mathbf{L^{I}}$ ligands were transformed in situ to the $\mathbf{L^{VI}}$ form, which has two different μ_4-bridging modes. In the first μ_4-bridging $\mathbf{L^{VI}}$ ligand, four of the carboxylate groups adopt the chelating mode. In the second $\mathbf{L^{VI}}$ ligand, three of the five *e*-carboxylate groups adopt the chelating mode and the *a*-carboxylate group adopts a monodentate mode (Figure 5b). The μ_4-$\mathbf{L^{VI}}$ ligands connect the Cd atoms to form a 2D porous layer lying in the *ac* plane, which is further extended through bridging 4,4′-bpy ligands to form a 3D coordination framework with 1D rectangular channels extending along the *b* axis (Figure 5c). It should be noted that the monodentate protonated 4,4′-Hbpy ligands extend into the rectangular channels and occupy the cavities. Only a little effective space is available for the lattice water molecules (Figure 5d).

A different structure, **6**, was obtained when the molar ratio of $Cd(NO_3)_2{\cdot}4H_2O$, $H_6\mathbf{L^{I}}{\cdot}H_2O$, and 4,4′-bpy was changed from 5:1:5 to 5:1:2 under similar reaction conditions at 175 °C. The $\mathbf{L^{I}}$ conformation was converted to the $\mathbf{L^{II}}$ form rather than the $\mathbf{L^{VI}}$ form as in **5**. X-ray crystal structure analysis showed there to be one crystallographically independent Cd atom, an $\mathbf{L^{II}}$ ligand that lies across a twofold axis, one monodentate protonated 4,4′-Hbpy, and ten disordered water molecules in the structural unit. Cd1 is coordinated by four oxygen atoms from the carboxylate groups and two monodentate monoprotonated 4,4′-Hbpy ligands in a distorted octahedral environment (Figure 6a). The $\mathbf{L^{II}}$ ligands adopt a μ_6-bridging mode through two monodentate and four chelating carboxylate groups, connecting the Cd atoms into a 2D coordination layer that lies in the *ac* plane (Figure 6b). To achieve charge balance in such a weakly acidic environment, the non-coordinated nitrogen atom of the 4,4′-bpy ligand must be protonated, as is found in many other compounds.[11] The monodentate protonated 4,4′-Hbpy ligands are arranged vertically above and below the layer and link the adjacent layers into a 3D supramolecular network (Figure 6c) through hydrogen bonds between the protonated 4,4′-Hbpy and carboxylate groups (N2···O4*i* 2.711 Å, N2–H2N···O4*i* 128°, N2···O5*i* 2.893 Å, N2–H2N···O5*i* 136°; *i*: $-1/4+x$, $1/4-y$, $3/4+z$). All of the lattice water molecules are located in the channels along the *b* axis, forming multiple hydrogen bonds with the carboxylate groups.

On further decreasing the amount of the auxiliary ligand 4,4′-bpy, a similar reaction resulted in another new product complex, **7**, at higher temperature. The $\mathbf{L^{I}}$ ligand conformation is transformed to the $\mathbf{L^{VI}}$ form, similar to that found in **5**. To our surprise, no 4,4′-bpy was found to be included in the final structure of **7**, neither as a ligand coordinated to the metal center nor as a guest molecule within the channels. However, the presence of 4,4′-bpy in the reaction system is essential for the formation of complex **7**. Without 4,4′-bpy, only complex **3** was obtained. X-ray crystallography showed the structure of **7** to be a 3D condensed framework containing three crystallographically independent Cd atoms, one $\mathbf{L^{VI}}$ ligand, and three coordinated water molecules in the asymmetric unit. Cd1 and Cd2 adopt octahedral geometries, being coordinated by five carboxylate oxygen atoms and one water molecule (Cd–O 2.198(6)–2.460(5) Å), while Cd3 is in a distorted pentagonal-bipyramidal environment surrounded by six carboxylate oxygen atoms and one water

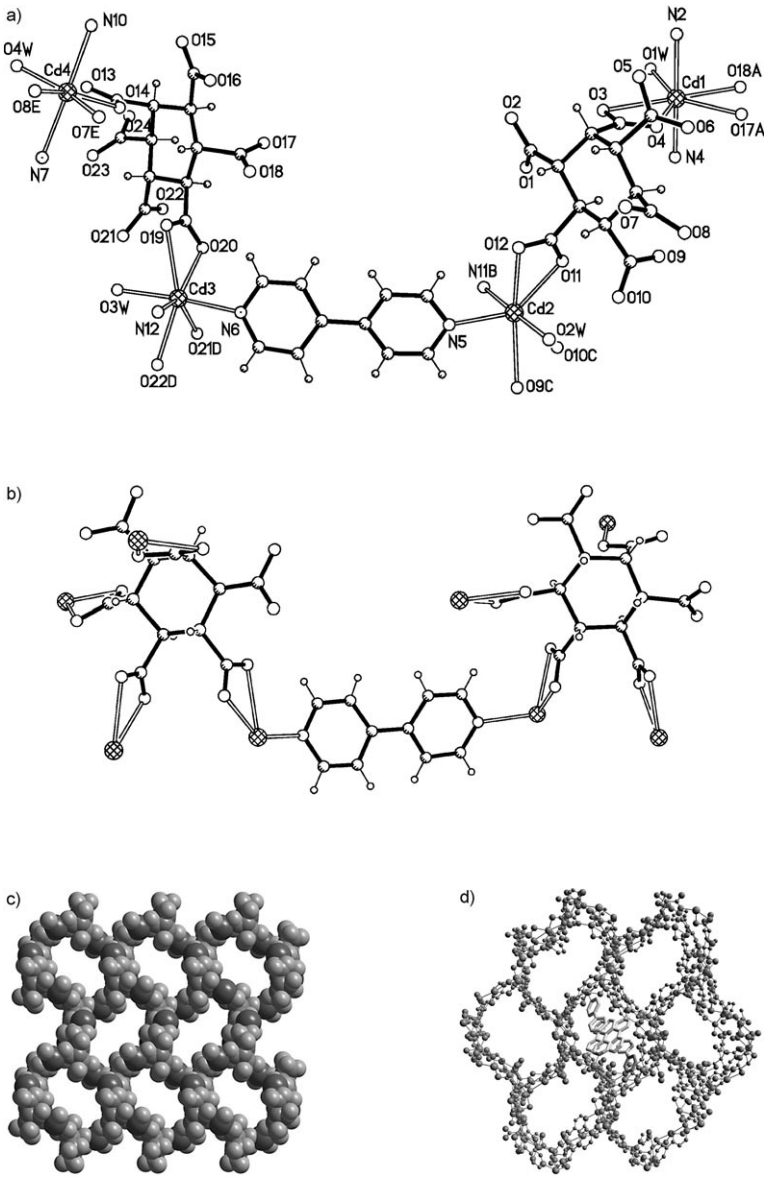

Figure 5. a) ORTEP drawing of the coordination environments of the Cd atoms with thermal ellipsoids at the 50% probability level. Perspective views of b) the coordination mode of the $\mathbf{L^{VI}}$ ligand, c) the 2D porous layer, and d) the 3D porous network filled with monodentate Hbpy along the *b* axis in **5** (some of the Hbpy molecules have been omitted for clarity).

molecule (Cd–O 2.260(5)–2.519(5) Å). The ligands in conformation $\mathbf{L^{VI}}$ adopt a μ_{11}-bridging mode, connecting eleven Cd atoms through five μ-η^1:η^1, μ-η^1:η^2, and μ-η^0:η^2 *e*-carboxylate groups and one distinct μ_3-η^1:η^2 *a*-carboxylate group (Figure 7a). A 3D ordered coordination framework is generated by the connection of μ_{11}-$\mathbf{L^{VI}}$ ligands and cadmium ions (Figure 7b).

3D magnetic metal-organic frameworks 8–11: When the paramagnetic metal ions Mn^{II}, Fe^{II}, and Ni^{II} were used instead of Cd^{II} ions, three isostructural 3D frameworks, **8**, **9**, and **10**, were formed under similar reaction conditions. Here, the structure of **8** is discussed in detail as a representative example. X-ray structural analysis revealed that **8** recrystallizes in the trigonal $R\bar{3}$ space group. The asymmetric unit contains one crystallographically unique Mn atom in a general position, one unique $\mathbf{L^{II}}$ ligand lying across a threefold axis, and two coordinated water molecules. Each Mn atom is coordinated in an octahedral geometry by four carboxylate oxygen atoms from three $\mathbf{L^{II}}$ ligands and two water molecules (Mn–O 2.153(2)–2.226(2) Å). Each $\mathbf{L^{II}}$ ligand connects nine Mn atoms through its six carboxylate groups in a *syn–anti* bridging mode (Figure 8a). A 3D metal-organic framework is thereby generated by the Mn–carboxylate coordination (Figure 8b). Moreover, if we neglect the cyclohexane rings, from the viewpoint of the magnetic superexchange pathway, each metal (M = Mn, Fe, Ni) atom is connected by four *syn–anti* μ-carboxylate bridges to form a 3D tetrahedrally connected M–M net. It should be noted that **8**–**10** are isostructural with our recently reported cobalt-**L** compound.[8b]

When the auxiliary ligands 2,2′-bpy or 4,4′-bpy are introduced into the reaction systems with Mn^{II} and Fe^{II} ions, the same phases of **8** and **9** are always obtained. This is also the case when 2,2′-bpy is added to the Ni-$\mathbf{L^{I}}$ reaction mixture and the same phase of **10** is formed. The 2,2′-bpy seems to have little influence on the construction of the frameworks in this specific reaction. However, when 4,4′-bpy is added to a mixture of nickel acetate and $H_6\mathbf{L^{I}}$, a new coordination framework, **11**, is formed.

X-ray crystallography has shown that the framework structure of **11** is constructed from chair-shaped tetranuclear $Ni_4(\mu_3\text{-}OH)_2$ secondary building units (SBUs), each of which is composed of four octahedral Ni atoms connected by two μ_3-OH groups (Ni1–O 2.055(4) Å and Ni2–O 2.040(4) Å). The octahedral coordination geometry of Ni1 is completed by three carboxylate oxygen atoms from different $\mathbf{L^{II}}$ ligands, one oxygen atom from the μ_3-OH, and one water molecule (Ni–O 2.018(4)–2.122(4) Å). Ni2 is surrounded by three carboxylate oxygen atoms from the $\mathbf{L^{II}}$ ligands, one μ_3-OH, one nitrogen atom from 4,4′-bpy, and one water mole-

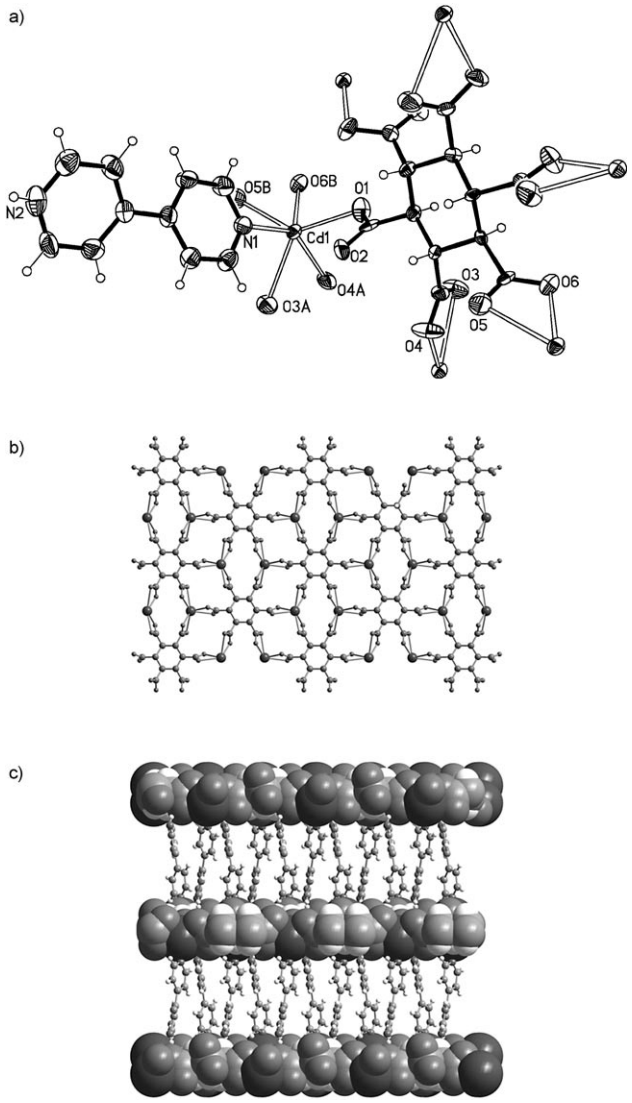

Figure 6. a) ORTEP drawing of the coordination environments of the Cd atoms and the coordination mode of the $\mathbf{L^{II}}$ ligand (with thermal ellipsoids at the 50% probability level), b) view of the 2D coordination layer, c) space-filling view of the 3D supramolecular network along the *b* axis in **6**.

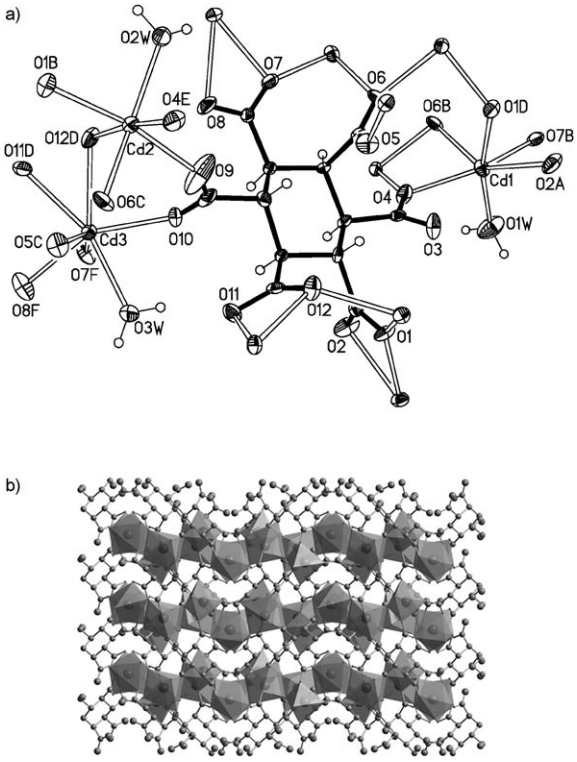

Figure 7. a) ORTEP drawing of the coordination environments of the Cd atoms and the coordination mode of the $\mathbf{L^{VI}}$ ligand with thermal ellipsoids at the 50% probability level, and b) perspective view of the 3D coordination network along the *a* axis in **7**.

cule (Ni–O 2.040(4)–2.115(4) Å, Ni-N = 2.060(5) Å) (Figure 9a). The ligand in conformation $\mathbf{L^{II}}$ adopts a μ_{10}-bridging mode connecting ten Ni atoms through six μ-η^1:η^1 and μ-η^0:η^2 *e*-carboxylate groups (Figure 9b). Each $Ni_4(\mu_3\text{-}OH)_2$ SBU links four $\mathbf{L^{II}}$ ligands and each $\mathbf{L^{II}}$ ligand connects to four tetranuclear SBUs (Figure 9c,d), resulting in a (4,4)-layer if the SBUs and $\mathbf{L^{II}}$ ligand are considered as four-connected nodes (Figure 9e,f). The 4,4′-bpy ligands coordinated to the Ni2 atoms bridge the layers to form a 3D coordination framework with 1D channels extending along the *c* axis (Figure 9g) and the *b* axis (Figure 9h). An analysis using PLATON[10] suggested that the channels occupy 44.9% of the crystal volume for **11**. The lattice water molecules are located within these channels, forming hydrogen bonds to the carboxylate groups. The calculated crystal density (in the absence of guests) of 1.280 $g\,cm^{-3}$ is comparable to those found for some low-density porous MOF materials.[12]

From a topological point of view, the 3D framework in **11** is a rare, elegant example of nets with four- and six-connected nodes. As pointed out by Öhrström and Larsson,[13a] nets with regular four (square-planar, tetrahedral, or trigonal prismatic)- and six (octahedral)-connected nodes are rare in the field of molecular-based nets, though the important nets with tetrahedral and octahedral nodes have long been known in inorganic-type structures, such as corundum (Al_2O_3). More particularly, all known MOF nets are based on more or less distorted tetrahedral and octahedral nodes.[13a] The network of **11** has an fsc topology,[13b] as shown schematically in Figure 9i). The long topological (O'Keeffe) vertex symbol is $4.4.4.4.6_2.6_2$ and $4.4.4.4.6_5.6_5.6_5.6_5.6_5.6_5.6_5.*.*.*$ for the square-planar and octahedral nodes, respectively, giving the short vertex symbol $(4^4.6^{10}.8)(4^4.6^2)$. To the best of our knowledge, only one example of the fsc topology has very recently been observed by Feng and co-workers in two intriguing isomeric $[(CuI)_7(DABCO)_{2.5}]$ (DABCO = 1,4-diazabicyclo[2.2.2]octane) frameworks.[13c] What interests us in particular is that the fsc topology is clearly different from the fsg net.[13a] The fsg net is a hypothetical net (of which no real example has yet been found) that has the same packing of the nodes as the primitive cubic packing (pcu) net but with two links removed per node in every second layer, which has the long topological

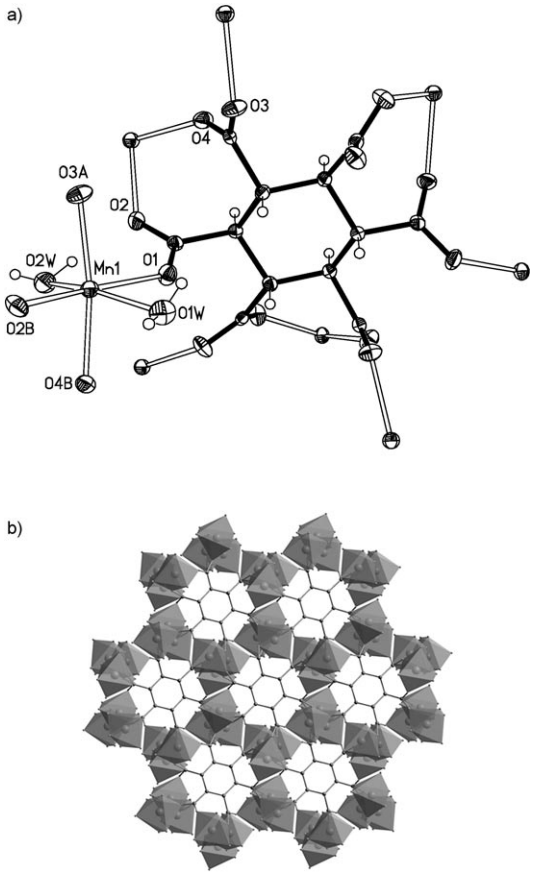

Figure 8. a) ORTEP drawing of the coordination environments of the Mn atoms and the coordination mode of the $\mathbf{L^{II}}$ ligand (with thermal ellipsoids at the 50% probability level), and b) polyhedron view of the 3D coordination network along the *c* axis in **8**.

(O'Keeffe) vertex symbol of $4.4.4.4.6_2.*$ and $4.4.4.4.4.4.4.4.6.6.6.6.6.*.*.*$ for the square-planar and octahedral nodes, respectively, giving the short vertex symbol $(4^4.6^2)(4^8.6^7)$. A related net with tetrahedral and octahedral nodes has previously been prepared by Batten and co-workers.[14c]

1D/2D Cu^{I}/Cu^{II} coordination polymers 12α and 12β: When the relatively active metal ion Cu^{II} was employed in the reaction system, two different phases, the 1D chain-based mixed-valence $Cu^{I,II}$ complex **12**α and the 2D layer-based porous framework **12**β, were obtained at the same time. X-ray crystal structure analysis of **12**α showed there to be two different parts in the asymmetric unit. One part is the Cu^{II} unit, which comprises one Cu^{II} atom, one unique $\mathbf{L^{II}}$ ligand lying across a twofold axis, and two coordinated water molecules. The other is the Cu^{I} unit, which comprises one Cu^{I} atom and one 4,4′-bpy ligand. The Cu^{II} atom adopts a tetragonal-pyramidal geometry, being coordinated by three carboxylate oxygen atoms from different $\mathbf{L^{II}}$ ligands and two water molecules (Cu^{II}–O = 1.940(2)–2.265(3) Å), while the Cu^{I} atom is in an almost linear geometry, being coordinated by two nitrogen atoms from the 4,4′-bpy ligands (Cu^{II}–N 1.907(3) and 1.910(3) Å) (Figure 10a). Notably, the N-Cu-N angle of 166.48(12)° is smaller than 180° due to a weak coordinating interaction between the Cu^{I} atom and two carboxylate oxygen atoms of the Cu^{II} unit (Cu^{I}–O 2.683 and 2.868 Å). The $\mathbf{L^{II}}$ ligands derived from $\mathbf{L^{I}}$ ligands adopt a μ_4-bridging mode through their monodentate carboxylate groups, linking the Cu^{II} atoms into a 1D chain that extends along the *a* axis (Figure 10b), while the 4,4′-bpy ligands also connect the Cu^{I} atoms to form a 1D chain along the *a* axis. Two Cu^{I}-4,4′-bpy chains are arranged on either side of the Cu^{II}–**L** chain to form a sandwich-like band structure through weak coordinating interactions between the Cu^{I} and the carboxylate groups (Figure 10c). A 3D supramolecular network is generated by π–π interactions and hydrogen bonds.

Complex **12**β is a layer-based framework containing one Cu^{II} atom, one monoprotonated $Hbtc^{2-}$ ligand generated in situ from the $\mathbf{L^{I}}$ ligand, one 4,4′-bpy, and one coordinated and three lattice water molecules (Figure 11a). The Cu^{II} atom is coordinated by two carboxylate oxygen atoms from different $Hbtc^{2-}$ ligands, two nitrogen atoms from two 4,4′-bpy ligands, and one aqua ligand in a tetragonal-pyramidal geometry (Cu^{II}–O 1.957(7)–2.303(8) Å, Cu^{II}–N 2.017(8) and 2.039(8) Å). The mixed μ_2-bridging $Hbtc^{2-}$ and 4,4′-bpy ligands connect the Cu^{II} atoms so as to form a 2D porous (4,4) grid layer (Figure 11b), which is further linked into a 3D supramolecular framework with two-dimensional channels extending along the directions of the *a* and *c* axes, respectively. These channels are occupied by lattice water molecules (Figure 11c).

Synthesis and ligand conformational transformation mechanism: In the rational design and synthesis of metal-organic coordination compounds, several factors should always be taken into consideration, such as the coordination properties of the metal ions, the functionality/flexibility/symmetry of the organic ligands, and the template effect of the structure-directing agents.[14] Small changes in one or more of these parameters can have a profound influence on the final products of the reaction. Complexes **1**–**7** were hydrothermally synthesized from Cd^{II} salts in the temperature range 130–180 °C under different reaction conditions, as summarized in Scheme 1. Complexes **1** and **2** are 3D frameworks with nanoscale cages that were obtained at 130 °C.[8c] The ligand **L** in **1** undergoes a conformational transformation from **I** to **II** in slightly acidic solution, while it converts from **I** to **II** and **III** in **2** in basic solution using NaOH to adjust the pH value. Notably, the same product, **2**, could also be obtained at 150, 160, and 180 °C. However, the use of other bases, such as LiOH, KOH, or Et_3N, in the above reaction system does not afford phase **2**, suggesting that the Na^{I} cation has an appropriate radius such that can act as a template in directing the construction of the 3D framework of **2**, thereby stabilizing the new intermediate conformation **III**. When a similar reaction was conducted without the addition of NaOH at a higher temperature of 180 °C, a 3D condensed framework of **3** was obtained, which has the same **II** conformation as observed in complex **1**.

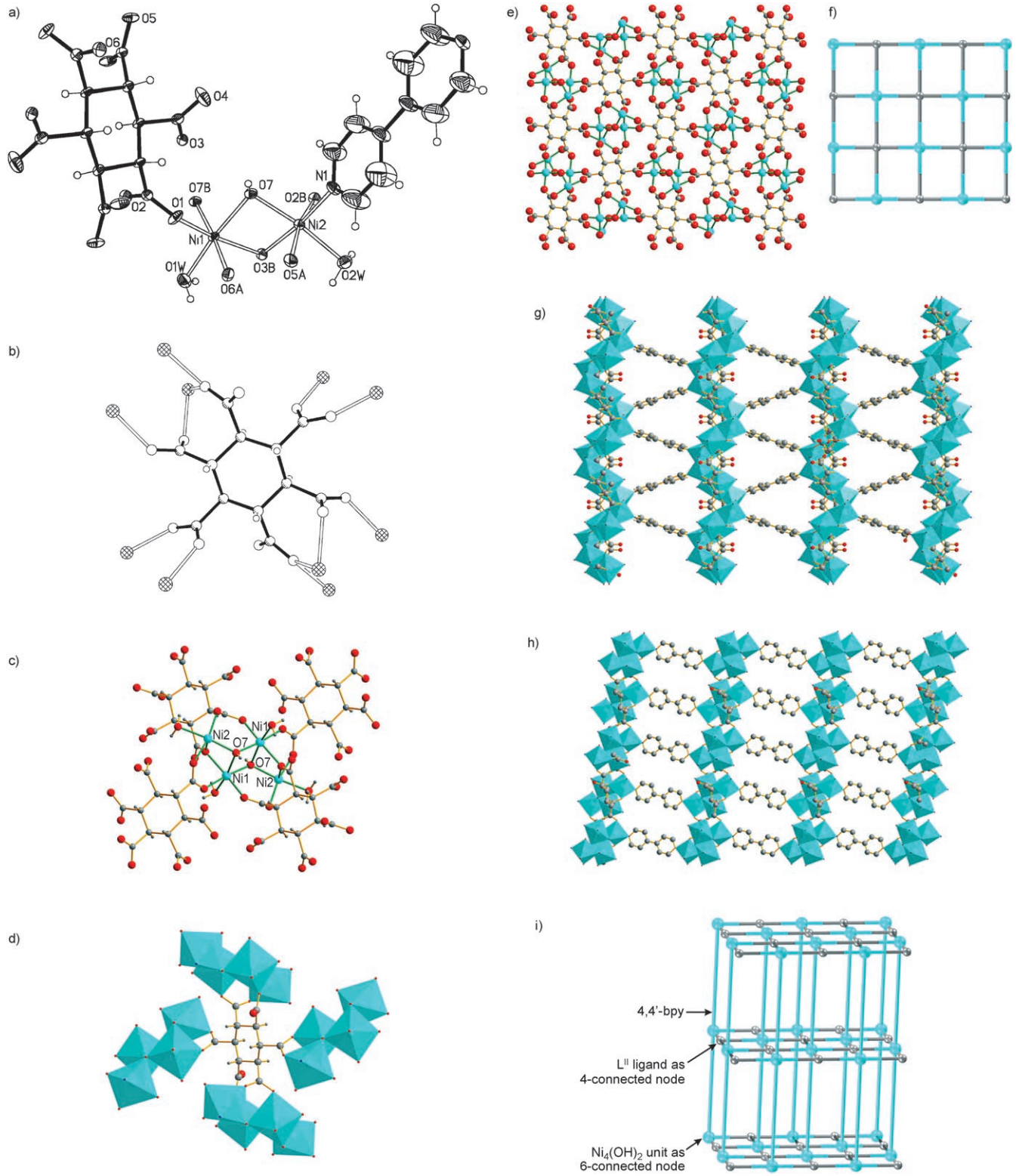

Figure 9. a) ORTEP drawing of the coordination environments of the Ni atoms (with thermal ellipsoids at the 50% probability level). Perspective views of b) the coordination mode of the $\mathbf{L^{II}}$ ligand, c) the 4-connected tetranuclear unit surrounded by four $\mathbf{L^{II}}$ ligands, d) the 4-connected $\mathbf{L^{II}}$ ligand surrounded by four tetranuclear clusters. Top views of e) the 2D coordination layer and f) the (4,4) topological layer. Polyhedron views of the 4,4′-bpy pillared 3D microporous framework along the g) *c* axis and h) *b* axis in **11**. i) The rare example of 3D binodal nets with square-planar and octahedral nodes in **11**. The pale-grey spheres represent $\mathbf{L^{II}}$ ligands as the 4-connected nodes, while the light-green spheres represent the centers of mass of $Ni_4(OH)_2$ units as the 6-connected nodes. The 4,4′-bpy ligands are represented by light-green bold lines.

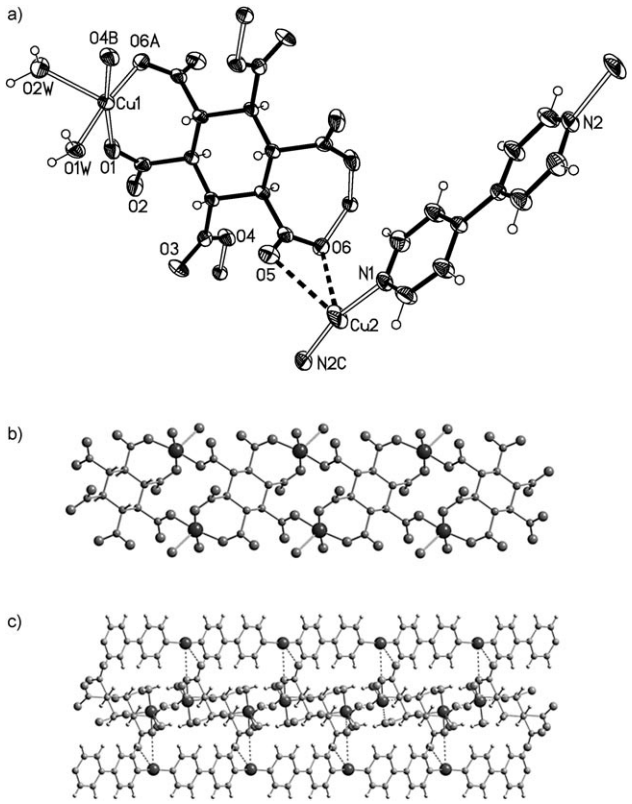

Figure 10. a) ORTEP drawing of the coordination environments of the Cu atoms and the coordination mode of the $\mathbf{L^{II}}$ ligand (with thermal ellipsoids at the 50% probability level). Perspective views of b) the 1D Cu^{II}-**L** chain, and c) the sandwich chain composed of two Cu^{I}-bpy chains and one Cu^{II}-**L** chain along the *a* axis in **12α**.

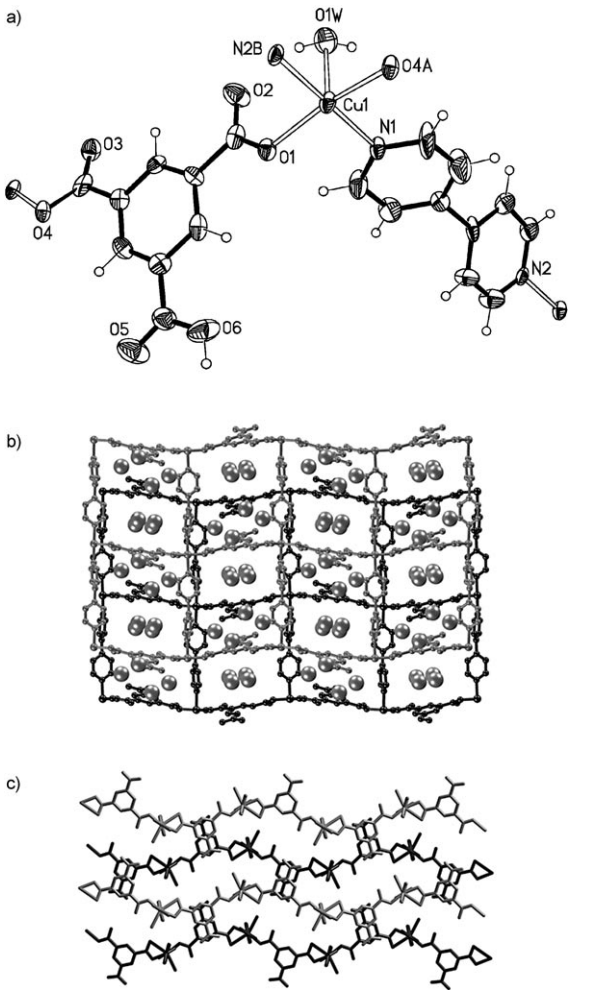

Figure 11. a) ORTEP drawing of the coordination environment of the Cu atom and the coordination mode of the $Hbtc^{2-}$ ligand (with thermal ellipsoids at the 50% probability level). Perspective views of b) the 3D porous framework with lattice water molecules based on a 2D coordination layer along the *a* axis, and c) the arrangement of the 2D layers in *AB* fashion viewed along the *c* axis in **12β**.

The introduction of auxiliary N-donor ligands changes the coordination behavior of the metal ions towards the carboxylate groups and thus has a subtle influence on both molecular arrangement and framework packing, and possibly the ligand conformations as well. When the chelating ligand 2,2′-bpy was added to the reaction system, a 3D supramolecular framework of **4** was obtained, in which the conformation of **L** is transformed from **I** to **III** (4e+2a). The divergent bridging ligand 4,4′-bpy apparently has a more profound influence on the framework construction and ligand conformational conversion. The reactions of $Cd(NO_3)_2{\cdot}4H_2O$, $H_6\mathbf{L^I}{\cdot}H_2O$, and 4,4′-bpy in molar ratios of 5:1:5, 5:1:2, and 5:1:1 at 160–180 °C resulted in different frameworks of **5**, **6**, and **7**. Interestingly, the addition of different stoichiometries of 4,4′-bpy leads to different architectures, 3D coordination framework **5**, 3D supramolecular framework **6**, and 3D condensed framework **7**. Moreover, in the absence of 4,4′-bpy, it is not complex **7** with the $\mathbf{L^{VI}}$ conformation but complex **3** with the $\mathbf{L^{II}}$ conformation that is obtained, illustrating that the 4,4′-bpy ligand plays an important role in the formation of **7** and in determining the ligand conformation, even though it is not incorporated in the final framework. It should be noted that complexes **4**, **5**, and **7** with the $\mathbf{L^{III}}/\mathbf{L^{VI}}$ ligand conformation are obtained in very low yields, which may be due to the low conformational conversion rate from the $\mathbf{L^{II}}$ to the $\mathbf{L^{III}}/\mathbf{L^{VI}}$ forms. It is very difficult to separate the microcrystal phase from the powder in high yields.

Furthermore, when other metal ions such as Co^{II},[8b] Mn^{II}, Fe^{II}, and Ni^{II} were chosen to react with the ligand **L** at different temperatures, only the isostructural phases **8**, **9**, and **10** were obtained, which may be due to their stable condensed coordination frameworks. The introduction of the auxiliary ligand 4,4′-bpy in the reactions has almost negligible effect on the products obtained with Mn^{II} and Fe^{II}, while a new Ni-**L**-4,4′-bpy coordination framework **11** was obtained when 4,4′-bpy was added to the reaction mixture. Notably, all of the ligands **L** in these four complexes adopt the $\mathbf{L^{II}}$ conformation. Compared with complexes **8**–**11**, the large atomic radius and versatile coordination geometries of the Cd^{II} ion in compounds **1**–**7** may be helpful for the stabilization and separation of the various conformations of **L**.[7f]

Since so many conformations of the 1,2,3,4,5,6-cyclohexanehexacarboxylate ligands have been trapped in metal-or-

ganic framework structures under hydrothermal conditions, the question arose as to how this happened and by what reaction mechanism. According to the literature,[7e,f] the three conformations of 1,4-cyclohexanedicarboxylic acid (1,4-H_2chdc) can be interconverted in a reversible equilibrium. This may be because the α-protons attached to the 1,4-carbons of cyclohexane can be easily removed, which will accelerate the interconversion equilibrium between the different conformations.[15] However, this is only a hypothetical mechanism. The details of the reaction mechanism and intermediates need further clarification. It may be possible to trap and stabilize some of the proposed intermediates in crystalline states through coordination to metal ions or other supramolecular interactions, with appropriate selection and control of the reaction temperature, time, and medium.[16] Inspired by our previous work,[3,13] we chose the relatively reactive and catalytically active metal ion Cu^{II},[17] hoping to trap the intermediates of the conformational transformation through its coordination. As expected, the reaction of $Cu(OAc)_2{\cdot}H_2O$, $H_6\mathbf{L^I}{\cdot}H_2O$, and 4,4′-bpy in a molar ratio of 5:1:5 resulted in two different crystalline phases, green block-shaped crystals of **12**α and green prismatic crystals of **12**β. In **12**α, the conformation of the ligand **L** is transformed from the $\mathbf{L^I}$ to the $\mathbf{L^{II}}$ form, while in **12**β it is oxidized to 1,3,5-benzenetricarboxylate. The successful isolation of complexes **12**α and **12**β possibly provides some structural evidence for the proposed conformational transformation mechanism. As far as the conformations of the cyclohexanehexacarboxylate ligand are concerned, we speculate that the approach of a metal ion to **L** can activate the α-protons on the ligand, leading to their removal, with the formation a metastable state **L***, similar to benzenehexacarboxylate, under the hydrothermal conditions (Scheme 3). The carboxylate groups rapidly adopt their optimal positions and coordinate to the metal ions. The α-protons return to their corresponding positions to form the final conformation of the ligand **L** in the frameworks. The reaction mechanism for the formation of **12**β may differ from that leading to the other compounds **1**–**12**α and involve removal of the α-protons and rapid decarboxylation at the 1,3,5-positions of **L*** due to steric hindrance, leading to the formation of benzenetricarboxylate. Under such circumstances, Cu^{II} acts as an essential oxidant in the reaction, as illustrated previously.[3,4]

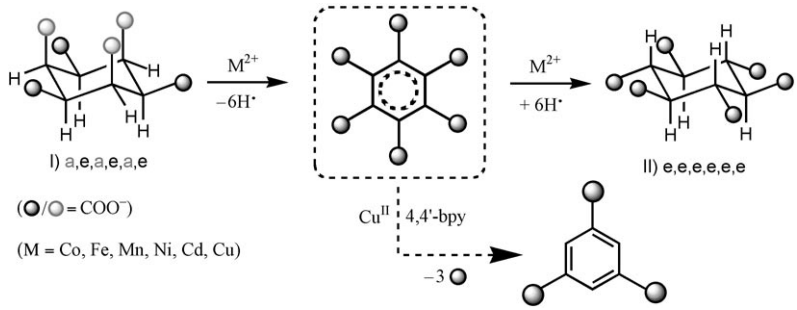

Scheme 3. Possible reaction mechanism of the conformational transformation of the $H_6\mathbf{L^I}$ ligand under hydrothermal conditions.

Thermogravimetric analysis: Thermogravimetric (TG) analyses were carried out to examine the thermal stabilities of the complexes **1**–**3** and **8**–**11**. Phase purity of the bulk materials was confirmed by comparison of their powder diffraction (XRPD) patterns with those calculated from single-crystal X-ray diffraction studies (Figure S1 in the Supporting Information). Samples were heated in air to 600 °C. Thermogravimetric analysis (TGA) of **1** showed that the lattice water molecules are removed in two steps (Figure 12a). The first weight loss of 5.4% between 20 and 120 °C corresponds to ten water molecules (calculated: 5.6%), and the second 4.0% weight loss between 120 and 170 °C corresponds to the remaining water molecules (calculated: 3.9%). The

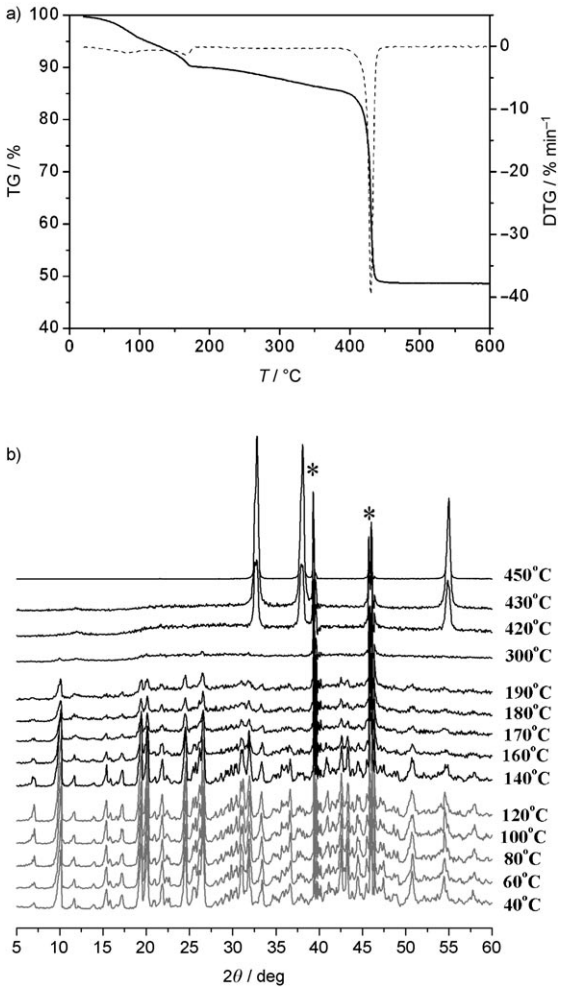

Figure 12. a) Thermogravimetric analysis (TGA) curves. b) Variable-temperature XRPD measurement of **1**.

twelve coordinated water molecules are gradually removed up to 400 °C (found: 6.5 %, calculated: 6.4 %). The framework starts to decompose on approaching 400 °C. The thermal stability was also confirmed by variable-temperature XRPD measurements (Figure 12b). Between 70 and 170 °C, the diffraction intensity of most peaks decreases, but the positions of the peaks remain the same upon gradual release of the guest water molecules, indicating that the framework remains intact. In comparison, the TGA curve of **2** (Figure 13a) indicates that the water molecules coordinated to

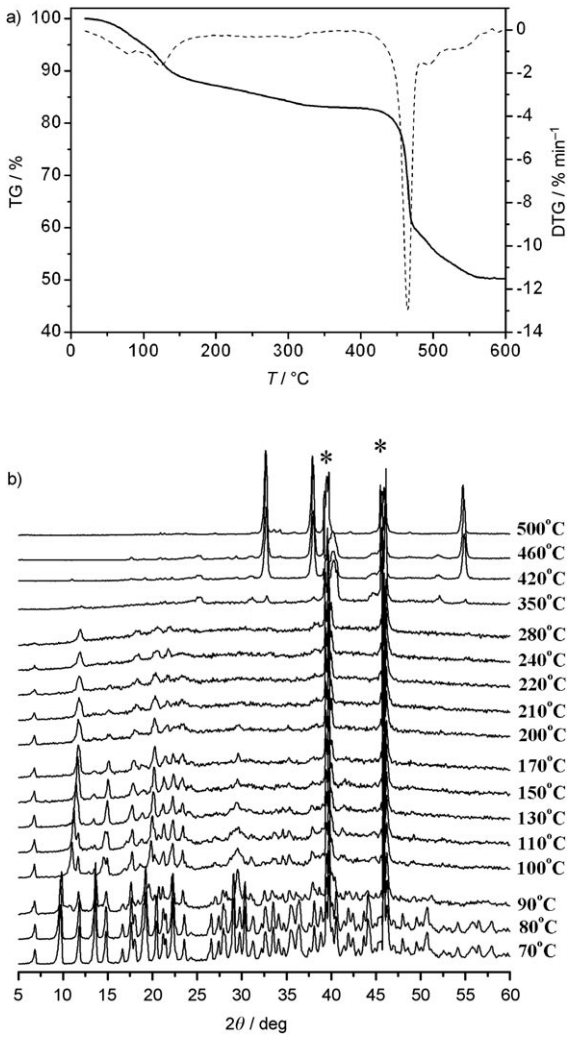

Figure 13. a) Thermogravimetric analysis (TGA) curves. b) Variable-temperature XRPD measurement of **2**.

Na^{I} are removed in a stepwise manner at up to 415 °C, and that the MOF begins to decompose beyond 460 °C. Variable-temperature XRPD measurements (Figure 13b) showed that there is an apparent shift for the sharp diffraction peaks from 10 to 12° upon the removal of about seven water molecules at 100 °C. This may be attributed to a local deformation of the coordination environments of the Cd atoms as a result of enhanced Na–carboxylate coordination when the water ligands coordinated to Na^{I} are gradually released from the cages. Most diffraction peaks persisted up to 280 °C, after which the mother framework began to collapse. In contrast to the former two porous complexes, **3** is a highly stable condensed framework. No coordinated water molecule was removed up to 350 °C, and the framework began to decompose at around 400 °C (Figure 14). Complexes **8**–**10** have the same framework connectivity and similar thermal stabilities (Figure 15a–c). Only complex **8** is discussed here. A rapid weight loss of 14.5 % between 155 and 265 °C and a slower loss of 2.9 % between 265 and 415 °C are in accordance with the loss of six coordinated water molecules per formula unit (calculated: 17.6 %), while the ensuing weight loss from 420 °C corresponds to the removal of all of the organic components to yield MnO_2 (found: 41.3 %; calculated: 42.3 %). Complex **11** with lattice water molecules in the porous framework is less stable (Figure 15d). The first weight loss of 8.3 % between room temperature and 78 °C corresponds to the loss of the four lattice water molecules (calculated: 7.9 %). Four coordinated water molecules (calculated: 7.9 %) were gradually removed up to 180 °C, accounting for the second weight loss of 8.5 %. After a stable stage in the range 180 to 280 °C without any weight loss, the 3D porous framework decomposed completely beyond 370 °C.

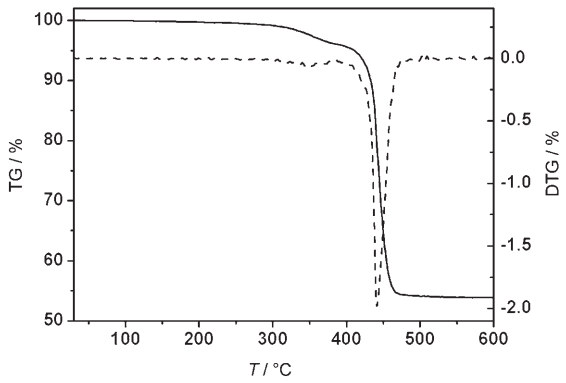

Figure 14. Thermogravimetric analysis (TGA) curve of **3**.

Magnetic properties: The magnetic properties of **8**–**11** were investigated over the temperature range 2–300 K (Figure 16). For **8**, the room temperature χT value per Mn^{II} ion is 4.297 $cm^3 mol^{-1} K$, which is close to the spin-only value (4.375 $cm^3 mol^{-1} K$). The $\chi(T)$ data in the range 20–300 K were fitted to the Curie–Weiss law $\chi(T) = C/(T-\theta)$ with a Weiss constant of $\theta = -9.04$ K and a Curie constant of $C = 4.48$ $cm^3 mol^{-1} K$ (Figure 16a), indicating a weak antiferromagnetic coupling between the Mn^{II} $S = 5/2$ spins through the *syn–anti* carboxylate bridges. Based on the 3D network connectivity (Figure 8b), only one effective magnetic exchange pathway is present within the net through the *syn–anti* carboxylate bridges, with the shortest Mn···Mn distance being 4.90 Å.

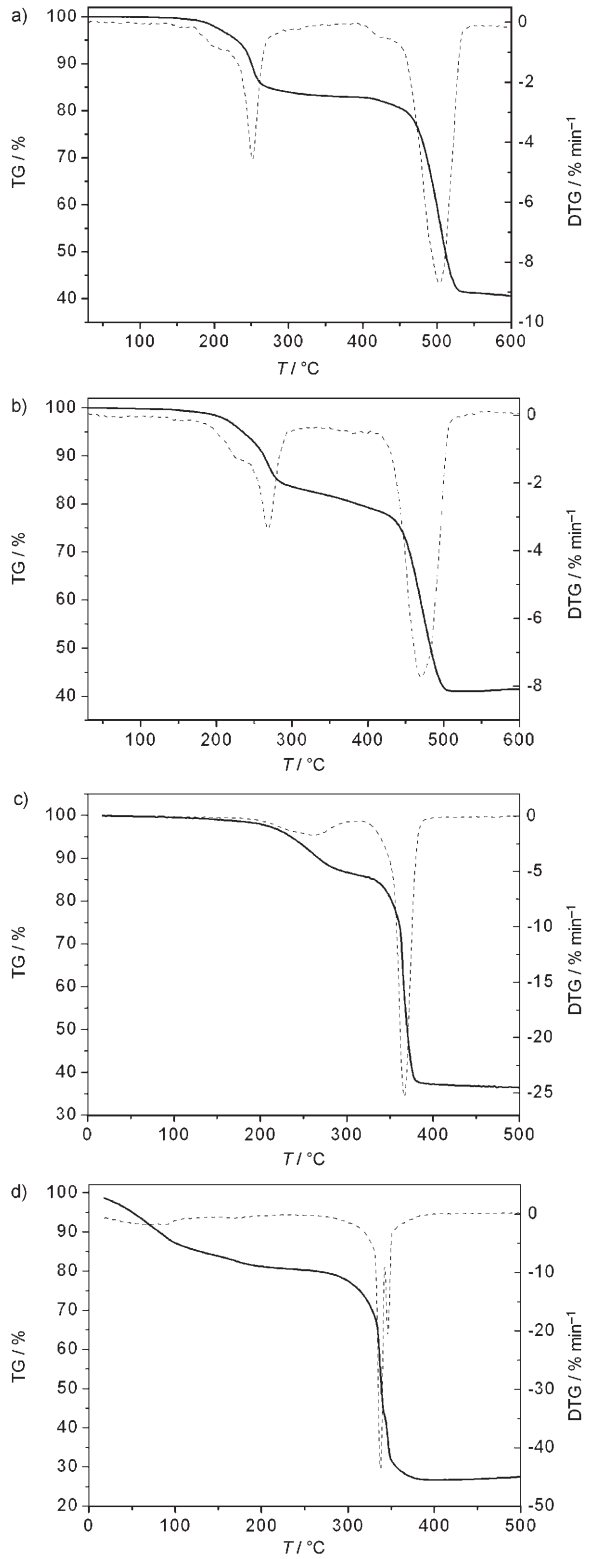

Figure 15. Thermogravimetric analysis (TGA) curves of a) **8**, b) **9**, c) **10**, and d) **11**.

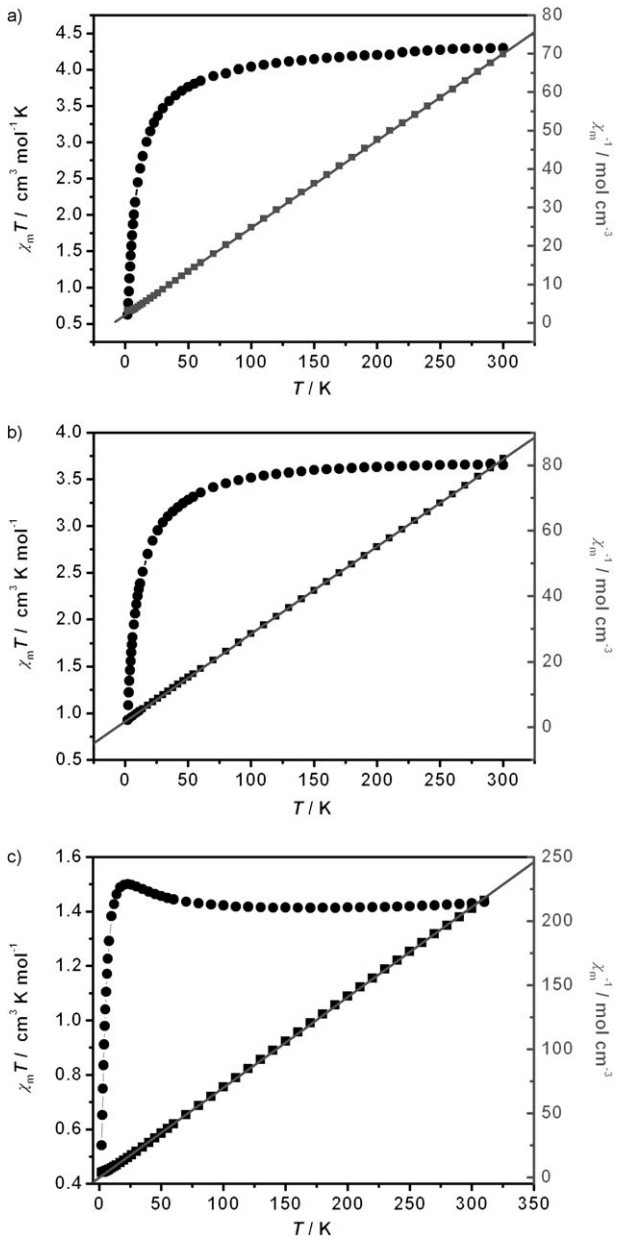

Figure 16. Temperature dependence of $\chi_M T$ (left) and χ^{-1} (right) for a) **8**, b) **9**, and c) **10**.

For **9**, the room temperature χT value per Fe^{II} ion is 3.654 $cm^3 mol^{-1} K$, which is close to the expected spin-only value (3 $cm^3 mol^{-1} K$) (Figure 16b). The $\chi(T)$ data in the range 10–300 K were fitted to the Curie–Weiss law $\chi T = C/(T-\theta)$ with a Weiss constant of $\theta = -6.64$ K and a Curie constant of $C = 3.75\ cm^3 mol^{-1} K$, indicating a relatively weak antiferromagnetic coupling between the Fe^{II} $S=2$ spins through the *syn–anti* carboxylate bridges, with the shortest Fe···Fe distance being 5.15 Å.

For **10**, the room temperature χT value per Ni^{II} ion is 1.43 $cm^3 mol^{-1} K$, which is slightly higher than the expected spin-only value (1 $cm^3 mol^{-1} K$) (Figure 16c). As T is lowered, $\chi_M T$ increases continuously to a maximum value of 1.50 $cm^3 mol^{-1} K$ at 23 K, and then rapidly decreases to a minimum value of 0.54 $cm^3 mol^{-1} K$, indicating weak ferromagnetic coupling between the Ni^{II} $S=1$ spins through the

syn–anti carboxylate bridges. The $\chi(T)$ data in the range 10–300 K were fitted to the Curie–Weiss law $\chi(T) = C/(T-\theta)$ with a Curie constant of $C = 1.42\,\mathrm{cm^3\,mol^{-1}\,K}$ and a Weiss constant of $\theta = 0.46$ K. There is only one effective magnetic exchange pathway present within the 3D net through the *syn–anti* carboxylate bridges, similar to those found in **8** and **9**. However, complex **10** exhibits ferromagnetic exchange, which differs from complexes **8** and **9**, in which there are antiferromagnetic interactions. This may be because the *syn–anti* carboxylate bridges can sometimes exchange ferromagnetic coupling.

Magnetic susceptibility versus temperature data (2–300 K) were collected at 0.2 T for **11**. The $\chi(T)$ data in the range 50–300 K were fitted to the Curie–Weiss law $\chi(T) = C/(T-\theta)$ with a Weiss constant of $\theta = -30.36$ K and a Curie constant of $C = 5.76\,\mathrm{cm^3\,mol^{-1}\,K}$. The room temperature χT value per Ni^{II}_4 unit is $5.24\,\mathrm{cm^3\,mol^{-1}\,K}$, which is slightly higher than the expected χT spin-only value ($4\,\mathrm{cm^3\,mol^{-1}\,K}$). As T is lowered, $\chi_M T$ decreases continuously to a value of $0.672\,\mathrm{cm^3\,mol^{-1}\,K}$, indicating a predominantly antiferromagnetic coupling in the structure. Notably, besides the μ_3-OH bridge, there are two other bridges between the Ni^{II} ions, the $\mathbf{L^{II}}$ carboxylate groups, and 4,4′-bpy ligands. The shortest Ni···Ni distance of two adjacent Ni^{II}_4 units through two carboxylate groups of **L** is 5.59 Å, which would be expected to permit very weak magnetic exchange coupling. The distance between two Ni^{II}_4 units across the 4,4′-bpy ligand is 16.67 Å.[18] Such a long separation precludes an efficient direct exchange between the Ni^{II} ions. Therefore, the antiferromagnetic interaction between Ni^{II} ions is expected to be through the μ_3-OH and μ_2-carboxylate groups within the chair-shaped tetranuclear $Ni_4(\mu_3\text{-OH})_2$ units, with Ni-O-Ni 93.72(14)°, and Ni-OH-Ni 96.60(15), 97.40(15), and 125.65(18)°, respectively, angles that are comparable to those in other tetranuclear $Ni_4(\mu_3\text{-OH})_2$ complexes.[19]

Based on the assumption that magnetic exchange should be negligibly small through both σ-type bonds of 1,2,3,4,5,6-cyclohexanehexacarboxylic acid and the long 4,4′-bipy bridge, a spin Hamiltonian was postulated for one tetranuclear unit with $S_i = 1$ for the Ni^{II} centers bridged by 4,4′-bpy ligands according to Equation (1):

$$H = -J_1(\mathbf{S}_1\cdot\mathbf{S}_2 + \mathbf{S}_1\cdot\mathbf{S}_3 + \mathbf{S}_2\cdot\mathbf{S}_4 + \mathbf{S}_3\cdot\mathbf{S}_4) - J_2\mathbf{S}_2\cdot\mathbf{S}_3 + \mu_B\sum\mathbf{S}_i\cdot\mathbf{B}\cdot\mathbf{g}_i - zj\langle S_z\rangle_T\sum\mathbf{S}_{z,i} \quad (1)$$

where J_1 denotes the isotropic exchange constant between the Ni1–Ni2 centers, and J_2 denotes that for the Ni2–Ni3 centers (Figure 17a). The intermolecular interactions among the Ni_4 units were treated with the molecular-field parameter *zj*. The magnetic interactions in the Ni_4 unit result in 81 magnetic states labeled as $|\alpha SM>$ calculated in the coupled basis set using the irreducible tensor operators technique,[20] where α denotes the intermediate quantum numbers denoting the coupling path. The thermal average of spin projection was calculated by an iterative procedure as:

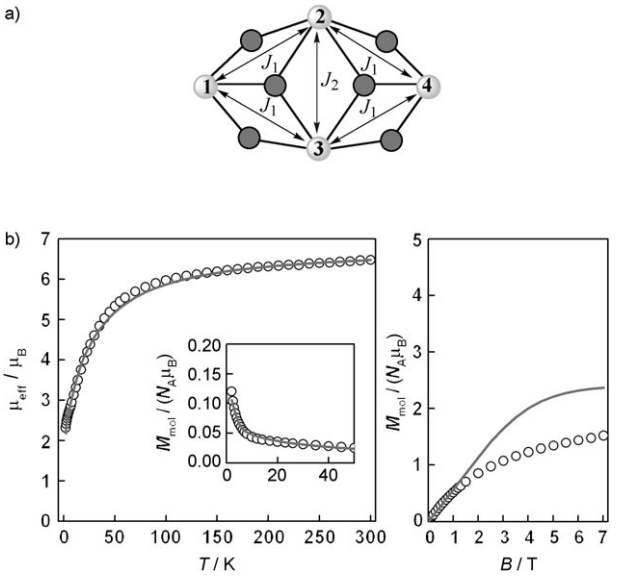

Figure 17. a) Scheme of the magnetic interactions among magnetic centers according to the spin Hamiltonian [Eq. (1)] for **11**. b) Left: temperature dependence of the effective magnetic moment (calculated from the magnetization at $B = 0.2$ T), with the low-temperature region expanded in the inset; right: field dependence of the magnetization at $T = 2$ K. ○: experimental data, ——: calculated data with the spin Hamiltonian and parameters in the text.

$$\langle S_z\rangle_T = \sum M\cdot\exp(-\varepsilon_i/kT)/\sum\exp(-\varepsilon_i/kT) \quad (2)$$

over all spin states and energy levels, resulting in:

$$\varepsilon_i = \varepsilon_{0,i}(\alpha S) + \mu_B g B M - zj\langle S_z\rangle_T M \quad (3)$$

where the first term corresponds to energy in zero magnetic field, the second is the Zeeman term, and the last term reflects the molecular-field correction. Finally, the molar magnetization was calculated according to Equation (4):

$$M_{mol} = -N_A\mu_B g\langle S_z\rangle_T \quad (4)$$

The best-fit parameters were found to be $J_1 = -11.5\ \mathrm{cm^{-1}}$, $J_2 = -16.3\ \mathrm{cm^{-1}}$, $g = 2.41$, and $zj/hc = -0.044\ \mathrm{cm^{-1}}$. The isotropic antiferromagnetic coupling in tetranuclear Ni^{II} unit adequately describes the magnetic behavior of **11** over the whole temperature range as well as the isothermal magnetization at $T = 2$ K up to $B = 1$ T (Figure 17b). Divergence in high magnetic fields can be ascribed to the polymeric character of the compound. The reconstructed energy levels are shown in Figure 18, with the ground state $S = 0$ and the first excited state $S = 1$ separated only by $1.9\ \mathrm{cm^{-1}}$. We have tried to improve the fitting by using 3-*J* parameters or adding ZFS parameters for Ni^{II}, but without any significant success.

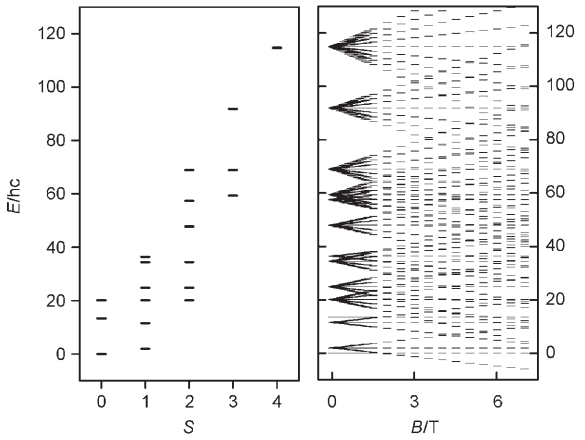

Figure 18. Reconstructed zero-field energy levels (left) and splitting of the energy levels in a magnetic field (right) for **11** using Eq. (1) and the parameters $J_1 = -11.5\ cm^{-1}$, $J_2 = -16.3\ cm^{-1}$, $g = 2.41$.

Conclusions

In summary, eleven new coordination polymers with various architectures have been prepared to trap the intermediate conformations of the ligand H_6**L** by tuning the reaction conditions of the hydrothermal synthesis. From the successful isolation of these complexes with different conformations, $\mathbf{L^{II}}$, $\mathbf{L^{III}}$ or $\mathbf{L^{VI}}$, the influence on the conformation of the ligand **L** may be summarized as follows: 1) metal ions with larger ionic radii and versatile coordination environments have a profound influence on the conformational conversions of H_6**L**. For example, $\mathbf{L^{II}}$, $\mathbf{L^{III}}$, and $\mathbf{L^{VI}}$ can be trapped in Cd complexes, while only $\mathbf{L^{II}}$ can be found in the Mn/Fe/Ni complexes; 2) alkali metal ions with suitable ionic radii may serve as structure-directing agents in the formation of metal-organic frameworks; basification of the reaction medium by the introduction of NaOH helps the conformational conversions of the organic ligands; and 3) the presence of the auxiliary ligands 2,2′-bpy/4,4′-bpy not only assists in the formation of coordination frameworks, but also has some subtle effects on the pH values of the solutions, which may accelerate the transformation of H_6**L** among all the various possible conformations and stabilize some *meso*-stable intermediate conformations. Furthermore, the formation of copper coordination polymers **12**α and **12**β may provide some structural clues to the conformational transformation mechanism of **L** involving the removal of the α-protons. This study not only demonstrates that the variable conformations of the ligand **L** play an important role in the construction of metal-organic frameworks, but also illustrates that the hydrothermal systems have a great effect on the conformational transformation, opening up a new way to study the variable conformations of flexible organic ligands.

Experimental Section

Materials and physical measurements: All of the starting materials employed were commercially available and were used as received without further purification. C, H, and N microanalyses were carried out with an Elementar Vario-EL CHNS elemental analyzer. FT-IR spectra were recorded in the range 4000–400 cm^{-1} from samples in KBr pellets on a Bio-Rad FTS-7 spectrometer. X-ray powder diffraction (XRPD) intensities were measured at 293 K on a Rigaku D/max-IIIA diffractometer ($Cu_{K\alpha}$, $\lambda = 1.54056$ Å) by scanning over the range 5–60° with a step size of $0.1°\,s^{-1}$. Variable-temperature XRPD measurements were made in the range 30–500 °C. Thermogravimetric (TG) analyses were carried out with a NETZSCH TG209F3 thermogravimetric analyzer; samples were heated from 20 to 600 °C at a rate of $10\,°C\,min^{-1}$.

Hydrothermal synthesis: All compounds were synthesized by a hydrothermal method.

$[Cd_{12}(\mu_6\text{-}L^{II})(\mu_{10}\text{-}L^{II})_3(\mu\text{-}H_2O)_6(H_2O)_6]\cdot 16.5H_2O$ (1): A mixture of $Cd(NO_3)_2\cdot 4H_2O$ (0.308 g, 1.0 mmol) and $H_6\mathbf{L^I}\cdot H_2O$ (0.087 g, 0.25 mmol) in H_2O (15 mL) was placed in a 25 mL Teflon reactor, which was sealed and heated in an oven at 130 °C for 60 h. The mixture was then cooled at a rate of about $5\,°C\,h^{-1}$ to give colorless block crystals of **1** as a single phase (in ca. 78% yield based on $H_6\mathbf{L^I}$). The crystals were isolated by filtration and washed with water. Elemental analysis calcd (%) for $C_{48}H_{81}O_{76.5}Cd_{12}$ (**1**): C 17.84, H 2.53; found: C 18.49, H 2.41; IR (KBr, 4000–400 cm^{-1}): $\tilde{\nu} = 3419$ (s), 2972 (w), 1608 (vs), 1402 (vs), 1333 (m), 1278 (w), 1204 (w), 1082 (w), 1039 (w), 936 (w), 794 (w), 739 (w), 579 (w), 524 (w), 493 cm^{-1} (w).

$Na_{12}[Cd_6(\mu_6\text{-}L^{II})(\mu_6\text{-}L^{III})_3]\cdot 27H_2O$ (2): Similarly to the synthesis of **1**, the hydrothermal reaction of $Cd(NO_3)_2\cdot 4H_2O$ (0.154 g, 0.5 mmol), $H_6\mathbf{L^I}\cdot H_2O$ (0.087 g, 0.25 mmol), and NaOH (0.080 g, 2.0 mmol) in water (15 mL) was performed at 130 °C or 180 °C for 72 h. Thereafter, the reaction mixture was cooled at a rate of about $5\,°C\,h^{-1}$ to give colorless prismatic crystals of **2** as a single phase (in ca. 82% yield based on $H_6\mathbf{L^I}$). Elemental analysis calcd (%) for $C_{24}H_{39}O_{37.5}Cd_3Na_6$ (**2**): C 20.55, H 2.80; found: C 20.48, H 2.66; IR (KBr, 4000–400 cm^{-1}): $\tilde{\nu} = 3415$ (s), 1593 (vs), 1399 (vs), 1305 (s), 1221 (w), 1192 (w), 1150 (w), 1073 (w), 1029 (w), 943 (w), 903 (w), 841 (m), 742 (w), 694 (w), 619 (w), 520 (w), 482 cm^{-1} (w).

$[Cd_3(\mu_{13}\text{-}L^{II})(\mu\text{-}H_2O)]$ (3): A mixture of $Cd(NO_3)_2\cdot 4H_2O$ (0.154 g, 0.50 mmol) and $H_6\mathbf{L^I}\cdot H_2O$ (0.087 g, 0.25 mmol) in H_2O (15 mL) was placed in a 25 mL Teflon reactor, which was sealed and heated in an oven to 180 °C for 72 h. The reaction mixture was then cooled at a rate of about $5\,°C\,h^{-1}$ to give colorless needle-like crystals of **3** as a pure phase (in ca. 52% yield based on Cd). The crystals were isolated by filtration and washed with water. The sample was allowed to dry in air, conditions under which it proved to be stable indefinitely. Elemental analysis calcd (%) for $C_{12}H_8O_{13}Cd_3$ (**3**): C 20.67, H 1.16; found: C 20.77, H 1.10; IR (KBr, 4000–400 cm^{-1}): $\tilde{\nu} = 3486$ (s), 3316 (s), 1607 (vs), 1563 (vs), 1405 (vs), 1331 (s), 1313 (s), 1198 (w), 1103 (w), 1075 (w), 934 (w), 865 (w), 807 (m), 784 (m), 759 (m), 726 (m), 579 (m), 553 (w), 517 cm^{-1} (w).

$[Cd_3(\mu_6\text{-}L^{III})(2,2'\text{-bpy})_3(H_2O)_3]\cdot 3.5H_2O$ (4): A mixture of $Cd(NO_3)_2\cdot 4H_2O$ (0.154 g, 0.50 mmol), $H_6\mathbf{L^I}\cdot H_2O$ (0.035 g, 0.10 mmol), and 2,2′-bpy (0.076 g, 0.5 mmol) in water (15 mL) was heated at 175 °C for 96 h. It was then cooled at a rate of about $5\,°C\,h^{-1}$. The resulting yellow lamellar microcrystals were mechanically separated to give a yield of **4** of about 15% (based on $H_6\mathbf{L^I}$). Elemental analysis calcd (%) for $C_{42}H_{43}O_{18.5}N_6Cd_3$ (**4**): C 39.88, H 3.43, N 6.64; found: C 39.51, H 3.31, N 6.92; IR (KBr, 4000–400 cm^{-1}): $\tilde{\nu} = 3390$ (s), 1580 (vs), 1475 (w), 1439 (w), 1399 (vs), 1315 (w), 1251 (w), 1156 (w), 1061 (w), 1017 (m), 930 (w), 896 (w), 770 (s), 736 (m), 650 (w), 610 (w), 504 cm^{-1} (w).

$[Cd_4(\mu_4\text{-}L^{VI})_2(4,4'\text{-Hbpy})_4(4,4'\text{-bpy})_2(H_2O)_4]\cdot 9.5H_2O$ (5): Similarly to the synthesis of **4**, hydrothermal reaction of $Cd(NO_3)_2\cdot 4H_2O$ (0.154 g, 0.50 mmol), $H_6\mathbf{L^I}\cdot H_2O$ (0.035 g, 0.10 mmol), and 4,4′-bpy (0.078 g, 0.5 mmol) in water (15 mL) was performed at 160 °C for 72 h. The mixture was then cooled at a rate of about $5\,°C\,h^{-1}$. The resulting colorless lamellar microcrystals were mechanically separated to give a yield of **5** of about 10% (based on $H_6\mathbf{L^I}$). Elemental analysis calcd (%) for $C_{84}H_{91}O_{37.5}N_{12}Cd_4$ (**5**): C 43.52, H 3.96, N 7.25; found C 43.12, H 4.13, N

7.07; IR (KBr, 4000–400 cm^{-1}): $\tilde{\nu}$ = 3391 (s), 2565 (m), 1933 (w), 1711 (s), 1603 (vs), 1490 (w), 1412 (vs), 1322 (m), 1243 (m), 1218 (m), 1149 (w), 1064 (m), 1043 (w), 1005 (m), 926 (w), 858 (w), 811 (s), 727 (w), 678 (w), 629 (s), 601 (w), 464 cm^{-1} (m).

$[Cd_2(\mu_6\text{-}L^{II})(4,4'\text{-Hbpy})_2]\cdot 10H_2O$ (6): Similarly to the synthesis of **4**, the hydrothermal reaction of $Cd(NO_3)_2\cdot 4H_2O$ (0.154 g, 0.50 mmol), $H_6\mathbf{L^I}\cdot H_2O$ (0.035 g, 0.10 mmol), and 4,4′-bpy (0.032 g, 0.2 mmol) in water (15 mL) was performed at 180 °C for 48 h. The mixture was then cooled at a rate of about 5 °C h^{-1} to give colorless prismatic microcrystals (in ca. 20 % yield based on Cd), which were mechanically separated. Elemental analysis calcd (%) for $C_{32}H_{44}O_{22}N_4Cd_2$ (**6**): C 36.21, H 4.18, N 5.28; found: C 36.57, H 4.01, N 5.61; IR (KBr) (4000–400 cm^{-1}): $\tilde{\nu}$ = 3399 (m), 3056 (w), 1600 (s), 1495 (w), 1410 (s), 1322 (m), 1245 (w), 1219 (m), 1071 (w), 1044 (w), 1012 (w), 935 (w), 806 (m), 728 (w), 629 (w), 566 (w), 493 cm^{-1} (w).

$[Cd_3(\mu_{11}\text{-}L^{VI})(H_2O)_3]$ (7): Similarly to the synthesis of **4**, the hydrothermal reaction of $Cd(NO_3)_2\cdot 4H_2O$ (0.154 g, 0.50 mmol), $H_6\mathbf{L^I}\cdot H_2O$ (0.035 g, 0.10 mmol), and 4,4′-bpy (0.032 g, 0.2 mmol) in water (15 mL) was performed at 180 °C for 72 h. The mixture was then cooled at a rate of about 5 °C h^{-1} to give colorless ellipsoidal microcrystals (in ca. 20 % yield based on $H_6\mathbf{L^I}$), which were carefully separated mechanically. Elemental analysis calcd (%) for $C_{12}H_{12}O_{15}Cd_3$ (**7**): C 19.65, H 1.65; found: C 19.47, H 1.58; IR (KBr, 4000–400 cm^{-1}): $\tilde{\nu}$ = 3203 (m), 1627 (s), 1567 (vs), 1409 (vs), 1319 (s), 1279 (m), 1245 (m), 1202 (w), 1067 (w), 932 (w), 800 (m), 754 (w), 724 (w), 674 (w), 633 (m), 566 (w), 503 (m), 442 cm^{-1} (w).

$[M_3(\mu_9\text{-}L^{II})(H_2O)_6]$ (M = Mn (8), Fe (9), and Ni (10)): A mixture of $MnCl_2\cdot 4H_2O$ (0.296 g, 1.50 mmol) (**8**) [or $FeCl_2\cdot 4H_2O$ (0.298 g, 1.50 mmol) (**9**) or $NiCl_2\cdot 6H_2O$ (0.356 g, 1.50 mmol) (**10**)], $H_6\mathbf{L^I}\cdot H_2O$ (0.174 g, 0.5 mmol), and NaOH (0.060 g, 1.5 mmol) in water (15 mL) was heated at 175 °C for 72 h. After cooling the mixture to room temperature over a period of approximately 14 h, colorless lamellar crystals of **8** were obtained, which were collected by filtration and washed with water (ca. 68 % yield based on $H_6\mathbf{L^I}$). Elemental analysis calcd (%) for $C_{12}H_{18}O_{18}Mn_3$ (**8**): C 23.43, H 2.95; found: C 23.46, H 2.94; IR (KBr, 4000–400 cm^{-1}): $\tilde{\nu}$ = 3494 (s), 3367 (s), 1616 (vs), 1559 (vs), 1410 (vs), 1316 (s), 1103 (w), 1080 (w), 923 (m), 820 (m), 758 (s), 585 (s), 516 cm^{-1} (s). Colorless prismatic crystals of **9** were obtained, collected by filtration, and washed with water (ca. 70 % yield based on $H_6\mathbf{L^I}$). Elemental analysis calcd (%) for $C_{12}H_{18}O_{18}Fe_3$ (**9**): C 23.33, H 2.94; found: C 23.28, H 2.97; IR (KBr, 4000–400 cm^{-1}): $\tilde{\nu}$ = 3487 (s), 3327 (s), 1614 (vs), 1559 (vs), 1404 (vs), 1315 (s), 1205 (w), 1103 (w), 931 (m), 757 (s), 689 (s), 576 (m), 522 cm^{-1} (s). Small green prismatic crystals of **10** were obtained, collected by filtration, and washed with water (ca. 46 % yield based on $H_6\mathbf{L^I}$). Elemental analysis calcd (%) for $C_{12}H_{18}O_{18}Ni_3$ (**10**): C 23.01, H 2.91; found: C 22.94, H 2.95; IR (KBr, 4000–400 cm^{-1}): $\tilde{\nu}$ = 3470 (s), 3332 (s), 1618 (vs), 1558 (vs), 1408 (vs), 1313 (s), 1198 (w), 1069 (w), 930 (m), 814 (s), 766 (s), 692 (s), 577 (m), 517 cm^{-1} (m).

$[Ni_4(\mu_3\text{-}OH)_2(\mu_{10}\text{-}L^{II})(4,4'\text{-bpy})(H_2O)_4]\cdot 6H_2O$ (11): A mixture of $Ni(OAc)_2\cdot 4H_2O$ (0.124 g, 0.5 mmol), $H_6\mathbf{L^I}\cdot H_2O$ (0.035 g, 0.1 mmol), and 4,4′-bpy (0.078 g, 0.5 mmol) in water (15 mL) was heated at 160 °C for 48 h. After cooling the mixture to room temperature over a period of ap-

Table 1. Crystal data and structure refinement for **1**–**9**, **11**, **12**.

	1 (293 K)	**2** (123 K)	**3** (293 K)	**4** (293 K)
formula	$C_{48}H_{81}O_{76.5}Cd_{12}$	$C_{48}H_{78}O_{75}Cd_6Na_{12}$	$C_{12}H_8O_{13}Cd_3$	$C_{42}H_{43}O_{18.5}N_6Cd_3$
F_w	3230.93	2805.38	697.38	1265.02
crystal system	trigonal	trigonal	triclinic	triclinic
space group	$R\bar{3}$	$R\bar{3}c$	$P\bar{1}$	$P\bar{1}$
a [Å]	17.797(1)	26.010(1)	9.4682(8)	11.6554(13)
b [Å]	17.797(1)	26.010(1)	9.4906(8)	13.7508(15)
c [Å]	22.961(4)	20.854(2)	10.2626(9)	16.8522(19)
α [°]	90	90	111.866(1)	73.634(2)
β [°]	90	90	105.264(1)	76.216(3)
γ [°]	120	120	107.533(1)	85.141(3)
V [Å^3]	6298.2(12)	12217.9(11)	738.99(11)	2516.4(5)
Z	3	6	2	2
ρ_{calcd} [g cm^{-3}]	2.556	2.288	3.134	1.670
μ [mm^{-1}]	3.108	1.744	4.359	1.333
R_1 [$I>2\sigma(I)$][a]	0.0615	0.0427	0.0359	0.0854
wR_2 (all data)[b]	0.1049	0.1212	0.0884	0.2384
	5 (123 K)	**6** (293 K)	**7** (293 K)	**8** (293 K)
formula	$C_{84}H_{91}O_{37.5}N_{12}Cd_4$	$C_{32}H_{44}O_{32}N_4Cd_2$	$C_{12}H_{12}O_{15}Cd_3$	$C_{12}H_{18}O_{18}Mn_3$
F_w	2318.29	1061.51	733.42	615.08
crystal system	triclinic	orthorhombic	orthorhombic	trigonal
space group	$P\bar{1}$	$Fdd2$	$Pbca$	$R\bar{3}$
a [Å]	13.9187(15)	15.918(2)	12.3424(12)	14.557(1)
b [Å]	14.5613(15)	50.471(7)	13.2718(14)	14.557(1)
c [Å]	22.182(2)	10.1138(12)	19.268(2)	14.968(2)
α [°]	93.236(2)	90	90	90
β [°]	91.339(2)	90	90	90
γ [°]	91.661(2)	90	90	120
V [Å^3]	4485.3(8)	8125.4(19)	3156.2(6)	2746.8(4)
Z	2	8	8	6
ρ_{calcd} [g cm^{-3}]	1.717	1.735	3.087	2.231
μ [mm^{-1}]	1.034	1.137	4.099	2.139
R_1 [$I>2\sigma(I)$][a]	0.0767	0.0458	0.0427	0.0343
wR_2 (all data)[b]	0.1869	0.0937	0.0871	0.0836
	9 (293 K)	**11** (293 K)	**12**α (293 K)	**12**β (293 K)
formula	$C_{12}H_{18}O_{18}Fe_3$	$C_{22}H_{32}O_{22}N_2Ni_4$	$C_{16}H_{15}O_8N_2Cu_2$	$C_{19}H_{20}O_{10}N_2Cu$
F_w	617.81	911.34	490.38	499.91
crystal system	trigonal	monoclinic	triclinic	monoclinic
space group	$R\bar{3}$	$P2_1/c$	$P\bar{1}$	$P2_1/n$
a [Å]	14.434(1)	14.8156(14)	7.8519(9)	10.6030(5)
b [Å]	14.434(1)	11.0770(11)	10.0583(12)	20.0687(8)
c [Å]	14.785(2)	13.4336(13)	11.5646(13)	11.1036(4)
α [°]	90	90	78.173(2)	90
β [°]	90	99.046(2)	71.787(2)	91.032(3)
γ [°]	120	90	73.741(2)	90
V [Å^3]	2667.7(5)	2177.2(4)	825.94(17)	2362.33(17)
Z	6	2	2	4
ρ_{calcd} [g cm^{-3}]	2.307	1.390	1.972	1.406
μ [mm^{-1}]	2.520	1.774	2.628	0.978
R_1 [$I>2\sigma(I)$][a]	0.0343	0.0684	0.0361	0.0799
wR_2 (all data)[b]	0.0897	0.2037	0.0955	0.2503

[a] $R_1 = \Sigma||F_o|-|F_c||/\Sigma|F_o|$. [b] $wR_2 = [\Sigma w(F_o^2-F_c^2)^2/\Sigma w(F_o^2)^2]^{1/2}$.

proximately 14 h, green lamellar crystals of **11** were obtained, which were collected by filtration and washed with water (ca. 52% yield based on $H_6\mathbf{L^I}$). Elemental analysis calcd (%) for $C_{22}H_{32}O_{22}N_2Ni_4$ (**11**): C 29.00, H 3.54, N 3.07; found: C 28.79, H 3.42, N 3.17; IR (KBr, 4000–400 cm^{-1}): $\tilde{\nu}$ = 3415 (s), 1610 (vs), 1567 (vs), 1399 (vs), 1325 (m), 1263 (w), 1219 (w), 1064 (w), 883 (w), 865 (w), 820 (m), 781 (w), 615 (m), 534 cm^{-1} (w).

$[\{Cu^{II}_2(\mu_4\text{-}L^{II})(H_2O)_4\}\{Cu^{I}_2(4,4'\text{-bpy})_2\}]$ (12α) and $[Cu^{II}(Hbtc)(4,4'\text{-bpy})(H_2O)]\cdot 3H_2O$ (12β): A mixture of $Cu(OAc)_2\cdot H_2O$ (0.100 g, 0.5 mmol), $H_6\mathbf{L^I}\cdot H_2O$ (0.070 g, 0.2 mmol), and 4,4′-bpy (0.078 g, 0.5 mmol) in water (15 mL) was heated at 175 °C for 72 h. After cooling to room temperature over a period of approximately 14 h, green block-shaped crystals of **12**α (in ca. 5% yield) and green prismatic crystals of **12**β (in ca. 10% yield) were obtained in two different phases. The crystals were mechanically separated and washed with water. Elemental analysis calcd (%) for $C_{14}H_{10}O_4N_2Cu$ (**12**α): C 50.38, H 3.02, N 8.39; found C 50.27, H 3.15, N 8.35; IR (KBr, 4000–400 cm^{-1}) for **12**α: $\tilde{\nu}$ = 3479 (m), 3388 (m), 1609 (vs), 1542 (vs), 1394 (s), 1330 (w), 1263 (w), 1215 (w), 1096 (w), 928 (w), 872 (w), 820 (m), 766 (w), 721 (w), 617 (m), 555 cm^{-1} (w). Elemental analysis calcd (%) for $C_{19}H_{20}O_{10}N_2Cu$ (**12**β): C 45.65, H 4.03, N 5.60; found C 45.69, H 3.95, N 5.55; IR (KBr, 4000–400 cm^{-1}) for **12**β: $\tilde{\nu}$ = 3445 (m), 1704 (m), 1618 (vs), 1562 (m), 1412 (w), 1360 (vs), 1225 (w), 1086 (w), 1015 (w), 924 (w), 868 (w), 818 (m), 731 (m), 635 (m), 550 cm^{-1} (w).

X-ray crystallography: Diffraction intensities of **1**–**12** were collected on a Bruker Apex CCD area detector diffractometer ($Mo_{K\alpha}$, λ = 0.71073 Å). Absorption corrections were applied using the multiscan program SADABS.[21] The structures were solved by direct methods and refined with a full-matrix least-squares technique using the SHELXTL program package.[22] Anisotropic thermal parameters were applied to all non-hydrogen atoms. The organic hydrogen atoms were generated geometrically; the aqua hydrogen atoms were located from difference maps and refined with isotropic temperature factors. Crystal data as well as details of the data collection and refinements for **1**–**9**, **11**, and **12** are summarized in Table 1. It should be noted that complex **10** crystallized in very small crystals, with similar crystal parameters to those of complex **8**, which were too weak to be amenable to data collection on the Bruker Apex CCD area detector diffractometer. Comparison of the powder diffraction (XRPD) pattern of **10** with that calculated from the single-crystal study of **8** (Figure S1 in the Supporting Information) confirmed that these complexes are isostructural.

CCDC-603913 (**1**), 603914 (**2**), 679411 (**3**), 679412 (**4**), 679413 (**5**), 679414 (**6**), 679415 (**7**), 601818 (**8**), 601819 (**9**), 679416 (**11**), 679417 (**12**α), and 679418 (**12**β) contain the supplementary crystallographic data for this paper. These data can be obtained free of charge from The Cambridge Crystallographic Data Centre via www.ccdc.cam.ac.uk/data_request/cif.

Computational method: All of the structures were optimized using Becke's three-parameter hybrid functional (B3LYP) method[23–25] and the 6–31G(d,p) basis set.[26] The stable configurations of the compounds were confirmed by means of frequency analysis, whereby no imaginary frequency was found for any of the configurations at the energy minima. The sum of the electronic and thermal free energies was used to compare stability. All of the calculations were performed with the Gaussian 03 program package.[27]

Acknowledgements

This work was supported by the NSFC (No. 20525102), the National Basic Research Program of China (2007CB815305), the Scientific and Technological Project of Guangdong Province (04205405), and the Czech Ministry of Education, Youth and Sports (Grant No. MSM6198959218).

[1] A. J. L. Pombeiro, V. Y. Kukushkin, J. A. McCleverty, J. M. Thomas, *Comprehensive Coordination Chemistry II*, Elsevier-Pergamon, Amsterdam, **2004**.

[2] a) W. B. Lin, Z. Y. Wang, L. Ma, *J. Am. Chem. Soc.* **1999**, *121*, 11249–11250; b) O. R. Evans, R.-G. Xiong, Z.-Y. Wang, G. K. Wong, W.-B. Lin, *Angew. Chem.* **1999**, *111*, 557–559; *Angew. Chem. Int. Ed.* **1999**, *38*, 536–538; c) C. M. Liu, S. Gao, H.-Z. Kou, *Chem. Commun.* **2001**, 1670–1671.

[3] a) X.-M. Zhang, M.-L. Tong, X.-M. Chen, *Angew. Chem.* **2002**, *114*, 1071–1073; *Angew. Chem. Int. Ed.* **2002**, *41*, 1029–1031; b) J.-P. Zhang, S.-L. Zheng, X.-C. Huang, X.-M. Chen, *Angew. Chem.* **2004**, *116*, 208–211; *Angew. Chem. Int. Ed.* **2004**, *43*, 206–209; c) S. Hu, J.-C. Chen, M.-L. Tong, B. Wang, Y.-X. Yan, S. R. Batten, *Angew. Chem.* **2005**, *117*, 5607–5611; *Angew. Chem. Int. Ed.* **2005**, *44*, 5471–5475; d) M.-L. Tong, L.-J. Li, K. Mochizuki, H.-C. Chang, X.-M. Chen, Y. Li, S. Kitagawa, *Chem. Commun.* **2003**, 428–429.

[4] a) J.-K. Cheng, Y.-G. Yao, J. Zhang, Z.-J. Li, Z.-W. Cai, X.-Y. Zhang, Z.-N. Chen, Y.-B. Chen, Y. Kang, Y.-Y. Qin, Y.-H. Wen, *J. Am. Chem. Soc.* **2004**, *126*, 7796–7797; b) X.-M. Zhang, R.-Q. Fang, H.-S. Wu, *J. Am. Chem. Soc.* **2005**, *127*, 7670–7671; c) D. Li, T. Wu, X.-P. Zhou, R. Zhou, X.-C. Huang, *Angew. Chem.* **2005**, *117*, 4247–4250; *Angew. Chem. Int. Ed.* **2005**, *44*, 4175–4178.

[5] a) S. Kitagawa, R. Kitaura, S.-i. Noro, *Angew. Chem.* **2004**, *116*, 2388–2430; *Angew. Chem. Int. Ed.* **2004**, *43*, 2334–2375; b) B. F. Abrahams, S. R. Batten, H. Hamit, B. F. Hoskins, R. Robson, *Angew. Chem.* **1996**, *108*, 1794–1796; *Angew. Chem. Int. Ed. Engl.* **1996**, *35*, 1690–1692; c) M. J. Zaworotko, *Chem. Commun.* **2001**, 1–9; d) C. Janiak, *Dalton Trans.* **2003**, 2781–2804; e) R. J. Hill, D.-L. Long, N. R. Champness, P. Hubberstey, M. Schröder, *Acc. Chem. Res.* **2005**, *38*, 335–348.

[6] a) H. Li, M. Eddaoudi, M. O'Keeffe, O. M. Yaghi, *Nature* **1999**, *402*, 276–279; b) C. A. Williams, A. J. Blake, P. Hubberstey, M. Schröder, *Chem. Commun.* **2005**, 5435–5437; c) S. S. Y. Chui, S. M. F. Lo, J. P. H. Charmant, A. G. Orpen, I. D. Williams, *Science* **1999**, *283*, 1148–1150; d) E. Yang, J. Zhang, Z.-J. Li, S. Gao, Y. Kang, Y.-B. Chen, Y.-H. Wen, Y.-G. Yao, *Inorg. Chem.* **2004**, *43*, 6525–6527; e) M. Sanselme, J. M. Grenèche, M. Riou-Cavellec, G. Férey, *Chem. Commun.* **2002**, 2172–2173; f) S. M. Humphrey, P. T. Wood, *J. Am. Chem. Soc.* **2004**, *126*, 13236–13237; g) S. O. H. Gutschke, D. J. Price, A. K. Powell, P. T. Wood, *Angew. Chem.* **2001**, *113*, 1974–1977; *Angew. Chem. Int. Ed.* **2001**, *40*, 1920–1923; h) M.-L. Tong, S. Kitagawa, H. C. Chang, M. Ohba, *Chem. Commun.* **2004**, 418–419.

[7] a) G. Seeber, A. L. Pickering, D.-L. Long, L. Cronin, *Chem. Commun.* **2003**, 2002–2003; b) A. L. Pickering, G. Seeber, D.-L. Long, L. Cronin, *Chem. Commun.* **2004**, 136–137; c) J. Fielden, D.-L. Long, L. Cronin, *Chem. Commun.* **2004**, 2156–2157; d) S. Kitagawa, K. Uemura, *Chem. Soc. Rev.* **2005**, *34*, 109–119; e) Y.-J. Kim, D.-Y. Jung, *Chem. Commun.* **2002**, 908–909; f) W. Bi, R. Cao, D. Sun, D. Yuan, X. Li, Y. Wang, X. Li, M.-C. Hong, *Chem. Commun.* **2004**, 2104–2105; g) A. Thirumurugan, R. A. Sanguramath, C. N. R. Rao, *Inorg. Chem.* **2008**, *47*, 823–831; h) A. Thirumurugan, M. B. Avinash, C. N. R. Rao, *Dalton Trans.* **2006**, 221–228.

[8] a) J. Wang, S. Hu, M.-L. Tong, *Eur. J. Inorg. Chem.* **2006**, 2069–2077; b) J. Wang, L.-L. Zheng, C.-J. Li, Y.-Z. Zheng, M.-L. Tong, *Cryst. Growth Des.* **2006**, *6*, 357–359; c) J. Wang, Y.-H. Zhang, M.-L. Tong, *Chem. Commun.* **2006**, 3166–3168.

[9] E. L. Eliel, N. L. Allinger, S. J. Angyal, G. A. Morrison, *Conformational Analysis*, Wiley, New York, **1996**.

[10] A. L. Spek, *PLATON, A Multipurpose Crystallographic Tool*, Utrecht University, Utrecht, **2003**.

[11] a) P. J. Zapf, R. C. Haushalter, J. Zubieta, *Chem. Commun.* **1997**, 321–322; b) Y. Lu, Y.-G. Li, E.-B. Wang, L. Xu, R. Clérac, *Eur. J. Inorg. Chem.* **2005**, 1239–1244; c) Y. Lu, Y. Xu, E.-B. Wang, H. Lu, C.-W. Hu, L. Xu, *Cryst. Growth Des.* **2005**, *5*, 257–260; d) Z.-M. Sun, J.-G. Mao, Y.-Q. Sun, H.-Y. Zeng, C. Abraham, *Inorg. Chem.* **2004**, *43*, 336–341.

[12] a) O. M. Yaghi, M. O'Keeffe, N. W. Ockwig, H. K. Chae, M. Eddaoudi, J. Kim, *Nature* **2003**, *423*, 705–714; b) C.-J. Li, S. Hu, W. Li, Z.-Q. Lam, Y.-Z. Zheng, M.-L. Tong, *Eur. J. Inorg. Chem.* **2006**, 1931–1935.

[13] a) L. Öhrström, L. Larsson, *Molecule-Based Materials. The Structural Network Approach*, Elsevier, Amsterdam, **2005**; b) http://

okeeffe-ws1.la.asu.edu/RCSR/home.htm; c) M. Bi, G. Li, J. Hua, Y. Liu, X. Liu, Y. Hu, Z. Shi, S. Feng, *Cryst. Growth Des.* **2007**, *7*, 2066–2070; d) A. M. Kutasi, A. R. Harris, S. R. Batten, B. Moubaraki, K. S. Murray, *Cryst. Growth Des.* **2004**, *4*, 605–607.

[14] a) R. Kitaura, K. Seki, G. Akiyama, S. Kitagawa, *Angew. Chem.* **2003**, *115*, 444–447; *Angew. Chem. Int. Ed.* **2003**, *42*, 428–431; b) X.-H. Bu, W. Chen, S.-L. Lu, R.-H. Zhang, D.-Z. Liao, W.-M. Bu, M. Shionoya, F. Brisse, J. Ribas, *Angew. Chem.* **2001**, *113*, 3301–3303; *Angew. Chem. Int. Ed.* **2001**, *40*, 3201–3203; c) S. I. Stupp, P. V. Braun, *Science* **1997**, *277*, 1242–1248; d) X.-L. Wang, C. Qin, E.-B. Wang, Z.-M. Su, *Chem. Eur. J.* **2006**, *12*, 2680–2691; e) D.-R. Xiao, Y.-G. Li, E.-B. Wang, L.-L. Fan, H.-Y. An, Z.-M. Su, L. Xu, *Inorg. Chem.* **2007**, *46*, 4158–4166.

[15] a) R. Kuhn, A. Wassermann, *Helv. Chim. Acta* **1928**, *11*, 50–54; b) Z. Welvart, *Soc. Chim. 5 serie* **1964**, 2203–2206.

[16] J.-P. Zhang, Y.-Y. Lin, X.-C. Huang, X.-M. Chen, *J. Am. Chem. Soc.* **2005**, *127*, 5495–5506.

[17] E. C. Constable, *Metals and Ligand Reactivity*, VCH, Weinheim, **1996**.

[18] a) D.-R. Xiao, E.-B. Wang, H.-Y. An, Y.-G. Li, Z.-M. Su, C.-Y. Sun, *Chem. Eur. J.* **2006**, *12*, 6528–6541; b) L.-M. Zheng, X.-Q. Wang, Y.-S. Wang, A. J. Jacobson, *J. Mater. Chem.* **2001**, *11*, 1100–1105.

[19] a) V. V. Pavlishchuk, S. V. Kolotilov, A. W. Addison, M. J. Prushan, D. Schollmeyer, L. K. Thompson, T. Weyhermüller, E. A. Goreshnik, *Dalton Trans.* **2003**, 1587–1595; b) J.-X. Chen, M. Ohba, D.-Y. Zhao, W. Kaneko, S. Kitagawa, *Cryst. Growth Des.* **2006**, *6*, 664–668; c) V. Ovcharenko, E. Fursova, G. Romanenko, I. Eremenko, E. Tretyakov, V. Ikorskii, *Inorg. Chem.* **2006**, *45*, 5338–5350.

[20] R. Boča, *Theoretical Foundations of Molecular Magnetism*, Elsevier, Amsterdam, **1999**.

[21] G. M. Sheldrick, *SADABS 2.05*, University of Göttingen, Göttingen.

[22] *SHELXTL 6.10*, Bruker Analytical Instrumentation, Madison, **2000**.

[23] A. D. Becke, *J. Chem. Phys.* **1993**, *98*, 1372–1377.

[24] A. Görling, *Phys. Rev. A* **1996**, *54*, 3912–3915.

[25] P. Hohenberg, W. Kohn, *Phys. Rev.* **1964**, *136*, 864–869.

[26] G. A. Petersson, A. Bennett, T. G. Tensfeldt, M. A. Al-Laham, W. A. Shirley, J. Mantzaris, *J. Chem. Phys.* **1988**, *89*, 2193–2218.

[27] Gaussian 03 (Revision D.1), M. J. Frisch, G. W. Trucks, H. B. Schlegel, G. E. Scuseria, M. A. Robb, J. R. Cheeseman, J. A. Montgomery, Jr., T. Vreven, K. N. Kudin, J. C. Burant, J. M. Millam, S. S. Iyengar, J. Tomasi, V. Barone, B. Mennucci, M. Cossi, G. Scalmani, N. Rega, G. A. Petersson, H. Nakatsuji, M. Hada, M. Ehara, K. Toyota, R. Fukuda, J. Hasegawa, M. Ishida, T. Nakajima, Y. Honda, O. Kitao, H. Nakai, M. Klene, X. Li, J. E. Knox, H. P. Hratchian, J. B. Cross, V. Bakken, C. Adamo, J. Jaramillo, R. Gomperts, R. E. Stratmann, O. Yazyev, A. J. Austin, R. Cammi, C. Pomelli, J. W. Ochterski, P. Y. Ayala, K. Morokuma, G. A. Voth, P. Salvador, J. J. Dannenberg, V. G. Zakrzewski, S. Dapprich, A. D. Daniels, M. C. Strain, O. Farkas, D. K. Malick, A. D. Rabuck, K. Raghavachari, J. B. Foresman, J. V. Ortiz, Q. Cui, A. G. Baboul, S. Clifford, J. Cioslowski, B. B. Stefanov, G. Liu, A. Liashenko, P. Piskorz, I. Komaromi, R. L. Martin, D. J. Fox, T. Keith, M. A. Al-Laham, C. Y. Peng, A. Nanayakkara, M. Challacombe, P. M. W. Gill, B. Johnson, W. Chen, M. W. Wong, C. Gonzalez, J. Pople, Gaussian, Wallingford, CT, **2005**.

Received: March 10, 2008
Published online: July 10, 2008

